Scientific Report No. 85

TWO DIMENSIONAL ANALYSIS OF ONE-PORT AND TWO-PORT RECTANGULAR MICROSTRIP ANTENNAS

by

Abdelaziz Benalla and K.C. Gupta

May 1986

Electromagnetics Laboratory
Department of Electrical Engineering
University of Colorado
Campus Box 425
Boulder, Colorado 80309

This report is based on a M.S. Thesis submitted by A. Benalla in July 1985. The research work was supported partially by research contracts from the Department of Navy (No. N65030-84-C-0095) and from the Office of Naval Research (No. N00014-84-K-0349).

TWO DIMENSIONAL ANALYSIS OF ONE-PORT AND TWO-PORT RECTANGULAR MICROSTRIP ANTENNAS

Abstract

Application of the segmentation method (which is based on the two-dimensional analysis) to the analysis of rectangular microstrip antennas is considered in this thesis. Both a single feed and two-port antennas are considered. In this analysis the microstrip antenna is divided into multiport network segments, which are characterized by their impedance matrices. The segmentation method uses these impedance matrices to find the antenna characteristics such as input impedance , resonant frequency and radiated power.

The effects of microstripline feed discontinuity, which may cause the excitation of higher order evanescent modes, are accounted for by considering the transmission line as a rectangular planar segment. The analysis reported in this thesis shows that these feed discontinuity junction reactances have considerable effect on the antenna design.

Two-port patches are used as elements of a series fed array. It is found that the power transmitted to the second port can be controlled either by varying the relative locations of input and output ports along the non-radiating edges or by changing the antenna width.

Experiments reported in this thesis verify the design approach for one-port and two-port rectangular microstrip antennas.

CONTENTS

LIST OF TABLES

LIST OF FIGURES

CHAPTER

I. INTRODUCTION 1

1.1 Microstrip Antennas 1

1.2 Outline of the Present Work 2

II. TRANSMISSION LINE MODEL OF A RECTANGULAR MICROSTRIP ANTENNA 4

2.1 Transmission Line Representation 4

2.2 Radiation Conductance 4

2.3 Edge Susceptance 9

2.4 Transmission Line Model for Rectangular Patch with One Feed Port 12

2.5 Two-Port Transmission Line Model 16

III. TWO-DIMENSIONAL ANALYSIS OF RECTANGULAR MICROSTRIP ANTENNAS 23

3.1 Introduction 23

3.2 Z-Matrix of a Rectangular Planar Component . . . 25

3.3 Edge Admittance Matrix 33

3.4 Segmentation Method 33

3.5 Application of the Segmentation Method to Single Feed Antennas 37

3.6 Two-Port Microstrip Antenna 52

CHAPTER

IV. EXPERIMENTAL RESULTS 62

4.1 Measurement of the Dielectric Constant of the Substrate 62

4.2 Single Feed Patch 67

4.3 Two-Port Patch 81

V. CONCLUSION 93

REFERENCES 95

APPENDIX A 97

TABLES

TABLE

3.1 Effects of Feed Discontinuity on the Input Impedances . . . 43

3.2 Effects of Feed Discontinuity on the Average Voltage at the Radiating Edges 44

3.3 Effects of Open End Discontinuity on the Input Impedance 47

3.4 Comparison of Single Feed Patch Designs Based on Segmentation Method and Transmission Line Model 50

3.5 Comparison of Two-Port Patch Designs Based on Segmentation Method and Transmission Line Model 55

4.1 Effects of Tolerance in ε_r on Z_{in} and f_r 69

4.2 Effects of Tolerance in $(a-x_1)$ on Z_{in} and f_r 69

4.3 Effects of Tolerance in b on Z_{in} and f_r 71

4.4 Effects of Tolerance in x_1 on Z_{in} and f_r 71

4.5 Effects of Tolerance in h on Z_{in} and f_r 73

4.6 Comparison between Theoretical and Measured Dimensions of the Single Feed Patch 73

4.7 Comparison of Theoretical and Measured Z_{in}, f_r and $|S_{11}|$ 80

4.8 Effects of Tolerance in ε_r on Z_{in} and f_r 85

4.9 Effects of Tolerance in a on Z_{in} and f_r 85

4.10 Effects of Tolerance in x_1 on Z_{in} and f_r 86

4.11 Effects of Tolerance in x_2 on Z_{in} and f_r 86

4.12 Comparison between Theoretical and Measured Antenna Dimensions 90

4.13 Comparison between Theoretical and Measured Z_{in}, f_r and $|S_{11}|$ 90

FIGURES

FIGURE

2.1 Rectangular microstrip patch antenna 5

2.2 Equivalent transmission line of a rectangular microstrip antenna 5

2.3 Edge conductance of a rectangular microstrip antenna versus the normalized width 8

2.4 Edge susceptance of a rectangular microstrip antenna versus normalized width 11

2.5 Rectangular microstrip antenna with the feed located at the radiating edges 14

2.6 Equivalent transmission line model of the rectangular microstrip antenna fed at the radiating edge 14

2.7 A two-port rectangular microstrip patch antenna . . . 17

2.8 Equivalent transmission line of a two-port rectangular microstrip antenna 18

2.9 Multiport network representation of the equivalent transmission line model 18

3.1 A rectangular planar component with feed location . . 24

3.2 A rectangular planar component showing the width and orientation of port p and q 24

3.3 Comparison of the two series formulations for the computation of elements of Z-matrix 32

3.4 Multiport network representation of the edge-admittance segment 34

3.5 Two multiport network segments 36

3.6 Overall multiport network segment 36

3.7 Multiport network representation of a single feed rectangular microstrip antenna 38

FIGURE

3.8 Numbering of the ports for combining the transmission line and rectangular segments 41

3.9 Numbering of the ports for combining the edge admittance 41

3.10 Effects of feed discontinuity on the reflection coefficient along the transmission line length 46

3.11 Voltage distribution at the radiating edges 48

3.12 Impedance locus of a single fed rectangular microstrip antenna 51

3.13 A multiport network representation of two-port rectangular microstrip antenna 53

3.14 Impedance locus of a two-port rectangular microstrip antenna 56

3.15 Variation of transmitted power to port 2 with the relative location of external ports and the antenna length 59

3.16 Variation of transmitted power with antenna width b 61

4.1 A stripline ring resonator with coupling gaps 63

4.2 Planar circuits and antenna fabrication process . . . 65

4.3 Photograph of the fabricated ring resonator 66

4.4 Setup for measuring the resonant frequency of the stripline ring resonator 68

4.5 Single feed rectangular patch configuration 75

4.6 Variation of the reflection coefficient magnitude with frequency 76

4.7 Variation of the average voltage at the radiating edges versus frequency 77

4.8 Photograph of the fabricated single feed rectangular microstrip antenna 78

4.9 General setup for using the network analyzer 79

4.10 Comparison of theoretical and measured reflection coefficient magnitude 82

FIGURE

4.11 Two-port rectangular microstrip antenna 84

4.12 Variation of $|S_{11}|$, $|S_{21}|$, $|S_{22}|$ with frequency for a two-port rectangular microstrip antenna 88

4.13 Photograph of the fabricated two-port rectangular microstrip antenna 89

4.14 Variation of theoretical and measured $|S_{11}|$, $|S_{21}|$, $|S_{22}|$ with frequency 91

CHAPTER I

INTRODUCTION

1.1 Microstrip Antennas

The concept of microstrip antennas, which has resulted in the evolution of thin planar low cost radiating structures, was first proposed by Deschamp [1] as early as 1953. The research into microstrip antennas did not intensify until better photo-etch techniques and various types of substrates having a wide range of dielectric constants and low loss tangents have been developed.

The microstrip antenna is a thin metal strip or patch of finite dimensions on top of a dielectric layer backed by a ground plane. This antenna has numerous advantages such as light weight, low volume and planar configuration. The radiation from this antenna is due to the fringing fields at the open circuited ends. The dielectric constant of the substrate should be low (≤ 2.5), so as to enhance the radiation.

The most popular type of microstrip patch configuration is the half-wave rectangular microstrip antenna. The simplicity of this structure has made it the object of intensive investigation in order to predict its characteristics such as the radiation pattern, input impedance and the resonant frequency. The exact

mathematical solutions for this open structure are difficult to implement. From a practical point of view, a recourse to cut-and-try experimental iterations is needed. Most of the up to date available methods are discussed in [2]. One of the simplest methods uses the transmission line model, which in its simple form takes into account only the fundamental mode. The microstrip antenna can also be modeled as a resonant cavity with complex impedance boundaries imposed at the four antenna edges. These methods do not accurately model the effects of feed discontinuity.

Since heights of substrates used are much smaller than the wavelength, microstrip patch antennas can be analyzed using two-dimensional analysis. One of the methods based on this approach is the segmentation method which has been used in antenna design [3-5]. In this method the rectangular antenna is divided into segments characterized by the z-matrices. Then the segmentation method uses the z-matrices to compute the antenna characteristics, such as input impedance, radiated power, bandwidth and resonant frequency.

1.2 Outline of the Present Work

The objective of the present study is to develop a method of analysis that can:

(i) take into account the feed line junction reactances accurately, and

(ii) yield results for two port patches needed in series feed arrays.

The analysis method developed here is based on the used two-dimensional impedance Green function for rectangular patches and the segmentation method. This approach yields a unified analysis for the feed lines and the patch. The antenna structures analyzed here are fed by microstrip lines along the non-radiating edges. This allows a wide range of input impedance values to be achieved by varying the feed location. The transmission lines connected to the patch are also considered as planar components. The effect of higher order modes which can be excited due to the feed discontinuity is accounted for. The radiated power can be controlled either by changing the width of the antenna or by changing the relative location of the input and output ports of a two-port antenna.

This thesis is divided into five chapters. In the second chapter, a discussion of the available formulations for the edge admittance of a rectangular patch is presented. Then the use of the transmission line model for the analysis of single feed and two-port antennas is discussed. The results of this model are to be compared to those obtained by the two-dimensional analysis discussed in the third chapter. In the latter, an improvement in the computational efficiency is achieved by increasing the convergence of the series representing the element of z-matrices of a rectangular patch. In the fourth chapter, the results of the two-dimensional analysis are used to design two antennas for experimental verification of the method. The experimental measured results are compared to the theoretical ones. Concluding remarks are contained in chapter V.

CHAPTER II

TRANSMISSION LINE MODEL OF A RECTANGULAR MICROSTRIP ANTENNA

2.1 Transmission Line Representation

The transmission line model is the simplest model used for analyzing rectangular microstrip antennas [2]. It is widely used for the first order design because of its simplicity.

This model consists of a length of transmission line loaded by radiating edge admittance on each end. This representation is usually employed here to estimate the input impedance and resonant frequency of the rectangular microstrip antenna shown in Fig. 2.1. A lumped parallel R-C model for the edge admittance is used. The results obtained by this method are compared with the two-dimensional analysis in chapter III. Two configurations with one and two-port rectangular microstrip antennas are discussed.

2.2 Radiation Conductance

This section presents a discussion of the available formulations for the radiation conductance associated with the radiating edge of a rectangular microstrip patch. A comparison of results obtained from these formulas is also included. The most widely used formula is obtained by considering radiating

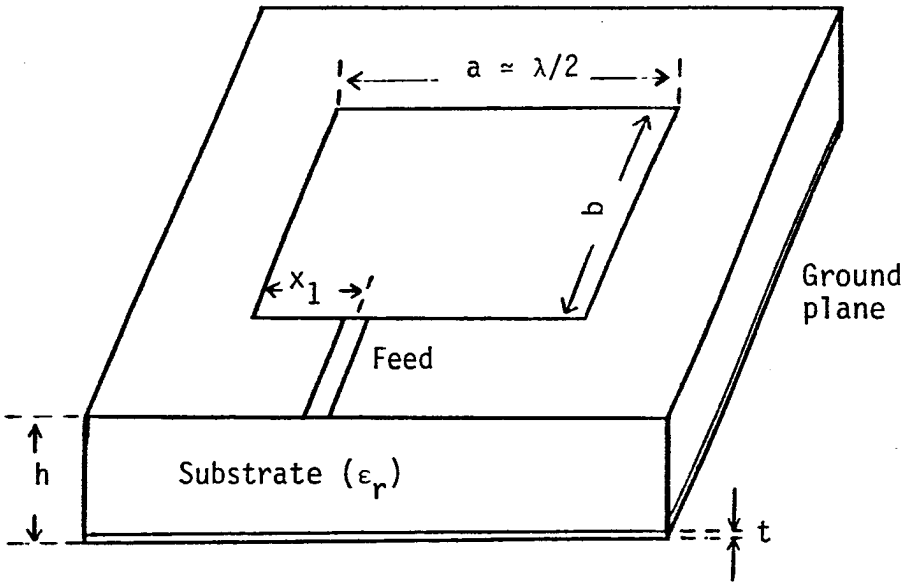

Figure 2.1 Rectangular microstrip patch antenna.

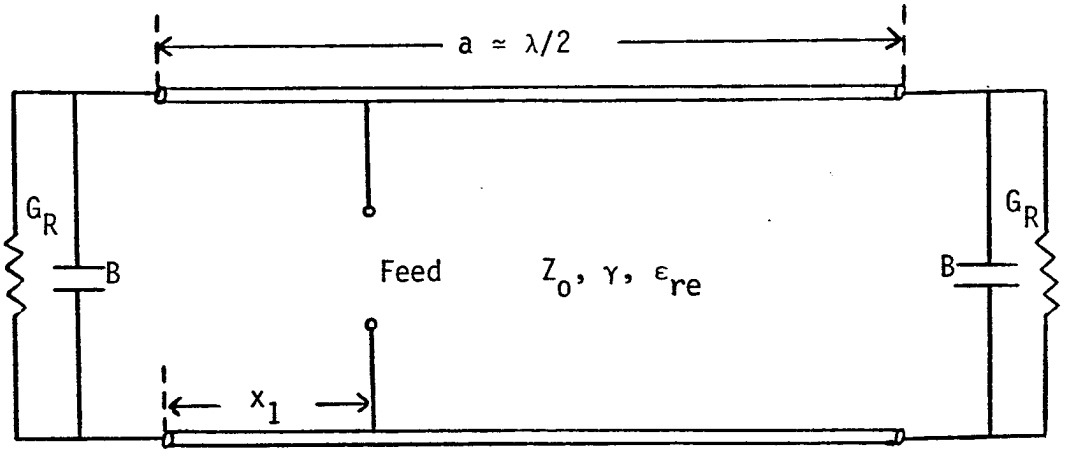

Figure 2.2 Equivalent transmission line of a rectangular microstrip antenna.

edges as slots radiating in half free space. As given by James et al. [6], this formula may be expressed as:

$$G_R = \begin{cases} \dfrac{b_e^2}{90\,\lambda_o^2} & b_e \le 0.35\,\lambda_o \\ \dfrac{b_e}{120\,\lambda_o} - \dfrac{1}{60\,\pi^2} & 0.35\,\lambda_o \le b_e \le 2\,\lambda_o \\ \dfrac{b_e}{120\,\lambda_o} & 2\,\lambda_o < b_e \end{cases} \qquad (2.1)$$

where λ_o is the free space wavelength and b_e is the effective width of the rectangular resonator of width b. G_R is the total radiation conductance (in mhos) associated with the radiating edge.

A more precise formula based also on the slot radiator model of the edge is given by Van de Capelle et al. [7] and may be expressed as

$$G_R = \frac{1}{\pi\eta_o}\left\{\left[k_o b_e \,si(k_o b_e) + \cos(k_o b_e) + \frac{\sin(k_o b_e)}{k_o b_e} - 2\right]\cdot\left[1 - \frac{(k_o h)^2}{24}\right] + \frac{(k_o h)^2}{12}\cdot\left[\frac{1}{3} + \frac{\cos(k_o b_e)}{(k_o b_e)^2} - \frac{\sin(k_o b_e)}{(k_o b_e)^3}\right]\right\} \qquad (2.2)$$

where η_o = free space wave impedance = $120\,\pi$, $k_o = 2\pi/\lambda_o$ and h is the height of the substrate.

$$si(x) = \int_0^x \frac{\sin(u)}{u}\,du\ .$$

The relation (2.2) is based on the assumption that the radiation from a rectangular antenna (Fig. 2.1) can be modelled by two rectangular slots with dimensions b_e and h in an infinite ground plane. Results based on these formulas are plotted in Fig. (2.3).

Two other formulas, useful for design and are based on Wiener Hopf characterization of a microstrip patch edge, are given by Kuester et al. [8] and Gogoi et al. [9] as:

The formula of Kuester et al. for electrically thin substrates ($k_0 h << 1$) may be written as:

$$G_R = \text{Real}\left[\frac{1 - e^{j\chi(0)}}{1 + e^{j\chi(0)}}\right] \tag{2.3}$$

where

$$\chi(0) = \frac{2k_0 h}{\pi\sqrt{\varepsilon_r}}\left\{\left[\ell n(jk_0 h) + \gamma - 1\right] + \varepsilon_r\left[2Q_0(-\delta_\varepsilon) - \ell n(2\pi)\right]\right\}$$

$$\delta_\varepsilon = \frac{\varepsilon_r - 1}{\varepsilon_r + 1}$$

$$Q_0(z) = \left(\frac{z}{1-z}\right)^2\left[\ell n\ 2 - Q_2(z)\right]$$

$$Q_2(z) = \sum_{m=1}^{\infty} z^m \ell n\left[\frac{(m+1)^2}{m(m+2)}\right], \quad |z| < 1$$

and $\gamma = 0.57721$ (Euler's constant)

The formula given by Gogoi et al. is as:

$$G_R = b_e \cdot \frac{7.75 + 2.2k_0 h + 4.8(k_0 h)^2}{1000\ \lambda_0} \cdot \left\{1 + \frac{(\varepsilon_r - 2.45)(k_0 h)^3}{1.3}\right\} \tag{2.4}$$

Accuracy of (2.4) is 1.1% for $0.05 \leq k_0 h < 0.6$ and $2.45 < \varepsilon_r < 2.65$. These two formulas are made accurate for wide patches (large value of b in Fig. 2.1). Results based on these formulas are also plotted in Fig. 2.3.

Fig. 2.3 shows a comparison of the formulas (2.1)-(2.4) for the following set of data: frequency, f = 7.5 GHz; dielectric

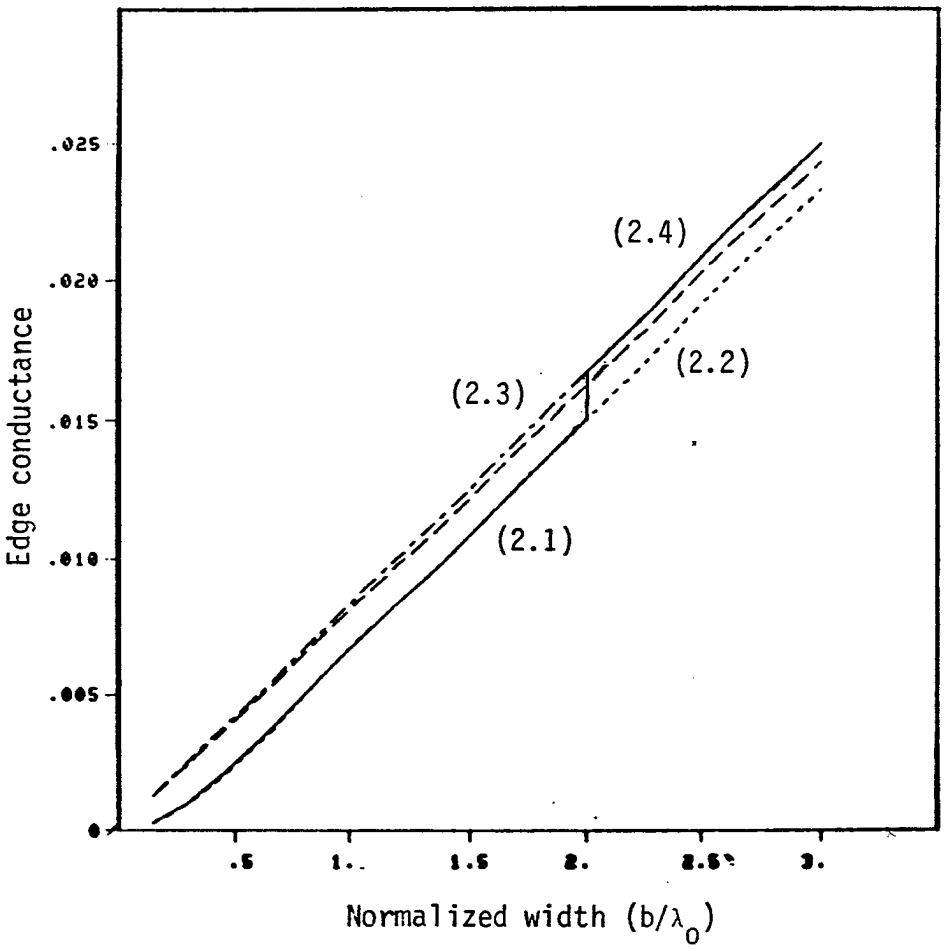

f = 7.5 GHz

ε_r = 2.48

h = 1/32 in.

Figure 2.3 Edge conductance of a rectangular microstrip antenna versus the normalized width.

constant $\varepsilon_r = 2.48$; and thickness of substrate, $h = 1/32$ in. It is inferred from Fig. 2.3 that formulas (2.1) and (2.2) yield close results as expected. The difference between formulas (2.1) and (2.4) increases with decreasing value of the width. This is because of the fact that (2.3) and (2.4) are valid only for wide patches. Formulas (2.3) and (2.4) are both based on the Wiener Hopf formulation and therefore yield identical results for all values of the width. From this limited discussion, it seems reasonable to use formula (2.1) due to its simplicity.

Although the power coupled to surface waves is very small compared to the radiated power, the conductance corresponding to the surface waves should be added to G_R. This conductance may be expressed as [9]

$$G_S = k_0 h\left[20.493 + 65.167\, k_0 h + 104.333(k_0 h)^2\right]10^{-4} \cdot b_e \left[1 + 3.5(\varepsilon_r - 2.45)(k_0 h)^3\right]/\lambda_0 \quad \text{mhos/m} \tag{2.5}$$

Accuracy of (2.5) is 2.6% for $0.2 < k_0 h < 0.6$ and $2.45 < \varepsilon_r < 2.65$.

2.3 Edge Susceptance

As discussed earlier, the fringing field effects can be accounted for by considering an edge susceptance (B) at the radiating edges. This susceptance needs to be known accurately for the computation of the resonant frequency. One of the formulas for B is based on the parallel plate waveguide model of a

microstrip and is given by [10] as:

$$B = \pi f \left\{ \frac{\sqrt{\varepsilon_{re}(a,h,t,\varepsilon_r)}}{cZ_o(a,h,t,\varepsilon_r)} - \frac{\varepsilon_o \varepsilon_r a}{h} \right\} b_e \tag{2.6}$$

where Z_o and ε_{re} are the characteristic impedance and effective dielectric constant of a microstrip line of width a. Expressions Z_o and ε_{re} are well known (see [11]). c is the velocity of waves in free space ($= 3 \times 10^8$ m/s). Another formula for B, which is based on open-end capacitance of a microstrip line [2], is igven by:

$$B = 0.01668 \cdot \frac{\Delta a}{h} \cdot \frac{b_e}{\lambda_o} \cdot \varepsilon_{re} \tag{2.7}$$

where

$$\frac{\Delta a}{h} = 0.412 \frac{(\varepsilon_{re}+0.3)(w/h + 0.264)}{(\varepsilon_{re}-0.258)(w/h + 0.8)} \tag{2.8}$$

Other formulas, which are based on the Wiener Hopf formulation and which can be used for wide patches, are given by Kuester et al. [8] and Gogoi et al. [9]. These are, respectively:

$$B = \text{imaginary} \left\{ \frac{1 - \exp(j\,\chi(0))}{1 + \exp(j\,\chi(0))} \right\} \tag{2.9}$$

where $\chi(0)$ was given by (2.3) and:

$$B = 0.01668 \frac{\Delta a}{h} \cdot \frac{b_e}{\lambda_o} \cdot \varepsilon_{re} \tag{2.10}$$

where

$$\frac{\Delta a}{h} = \frac{0.95}{1 + 0.85 k_o h} - \frac{0.075(\varepsilon_r - 2.45)}{1 + 10\, k_o h} \tag{2.11}$$

The accuracy of (2.13) is 2% for $0.1 < k_o h < 0.6$ and $2.45 < \varepsilon_r$

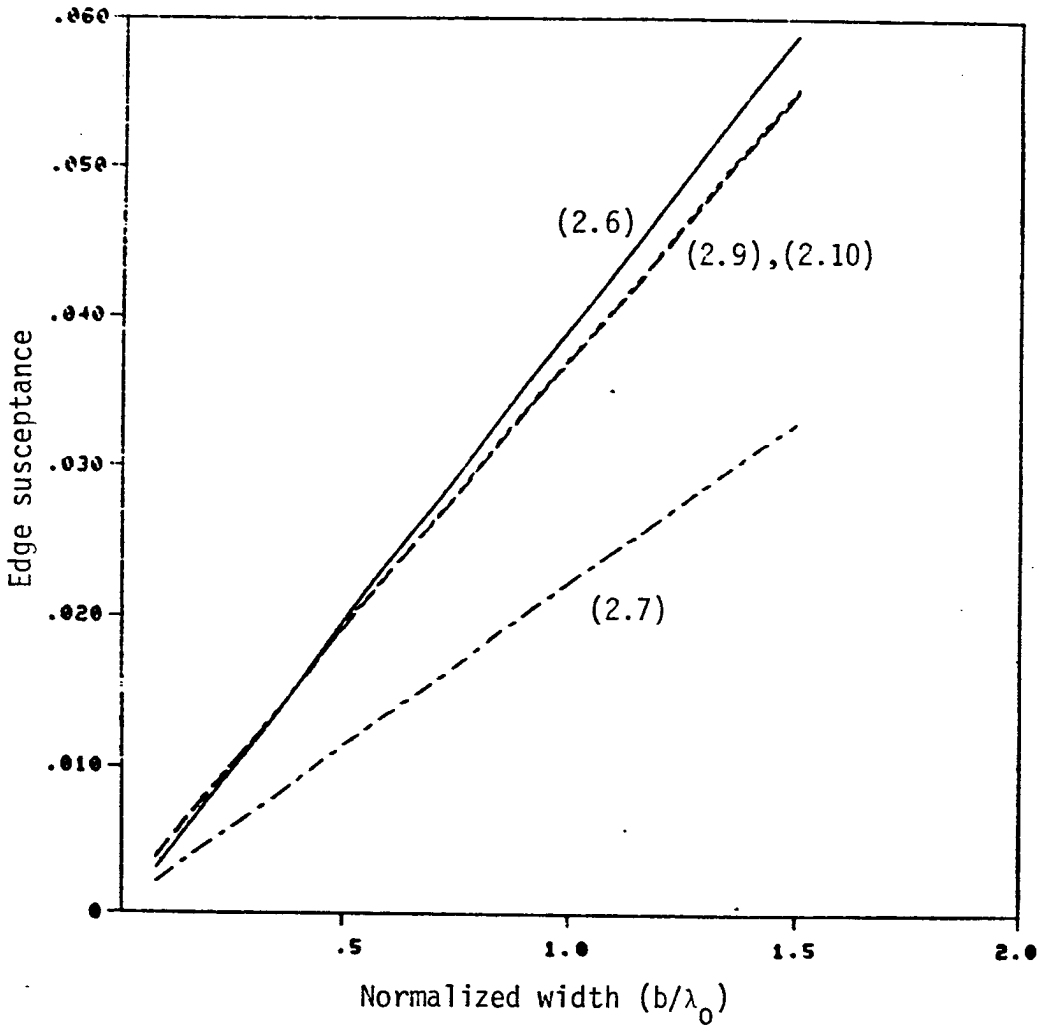

Figure 2.4 Edge susceptance of a rectangular microstrip antenna versus normalized width

< 2.65. Formulas (2.6) through (2.11) are compared in Fig. (2.4), expression (2.6), (2.7) and (2.10) give close results for all practical values of the resonator width ($0.25\ \lambda_0 \leq w \leq 0.6\ \lambda_0$). (2.7) predicts an end susceptance value of one-half of that computed using other formulas. For all practical values of interest, formula (2.6) may be used, since there is no restriction on the width of the patch for this formula. When the width is large both (2.9) and (2.10) can be used.

2.4 Transmission Line Model for Rectangular Patch with One Feed Port

The rectangular microstrip antenna of Fig. 2.1, can be modeled as a transmission line which is effectively $\lambda/2$ at resonance ($\lambda = \lambda_0/\sqrt{\varepsilon_{re}}$). The radiation occurs mainly from the edges which are $\lambda/2$ apart. This is incorporated into the model by loading the transmission line at both ends by an aperture conductance G_R as shown in Fig. 2.2. Power loss because of surface waves can also be added to in G_R. The effects of the fringing field at the open edges of the patch, are incorporated by terminating each end of the transmission line in an aperture capacitance represented by a susceptance B. Fringing fields at the other edges (of length a) are accounted for by taking an effective width b_e. Dielectric losses are considered by using a complex propagation constant γ. A more common practice is to construct a transmission line model with susceptance at radiating edges accounted for by extending the edges outwards, i.e. by increasing the effective length of the line. This version of a

transmission line model yields reasonable results as long as the extension is very small but is inaccurate to the extent that we are shifting the phase centers of the radiating slots outwards. At non-radiating edges no such error is involved by extending the edges outwards to account for the fringing field.

The input admittance at a distance x_1 from one of the edges of a microstrip antenna (fed along its length as shown in Fig. 2.2, or fed at the radiating edge ($x_1 = 0$) as shown in Fig. 2.5) is expressed as:

$$y_1 = y_{in1} + y_{in2} \tag{2.12}$$

where y_{in1}, y_{in2} are the edge admittances transformed by a distance x_1 and $(a-x_1)$ respectively and are expressed as:

$$y_{in1} = y_0 \frac{y_L \cosh(\gamma x_1) + y_0 \sinh(\gamma x_1)}{y_0 \cosh(\gamma x_1) + y_L \sinh(\gamma x_1)} \tag{2.13}$$

$$y_{in2} = y_0 \frac{y_L \cosh(\gamma x_2) + y_0 \sinh(\gamma x_2)}{y_0 \cosh(\gamma x_2) + y_L \sinh(\gamma x_2)} \tag{2.14}$$

where $\gamma = j\omega\sqrt{\mu\varepsilon_{re}(1-j\delta)}$, $x_2 = a-x_1$, δ is the dielectric loss tangent y_0 is the characteristic admittance of the line.

The effects of the parasitic reactances at the feed point (which arises from the higher order modes excited due to discontinuity) are approximately accounted for by a series inductive reactance given by [2]

$$x_L = \frac{377}{\sqrt{\varepsilon_{re}}} \tan\left(\frac{2\pi h}{\lambda_0}\right) \tag{2.15}$$

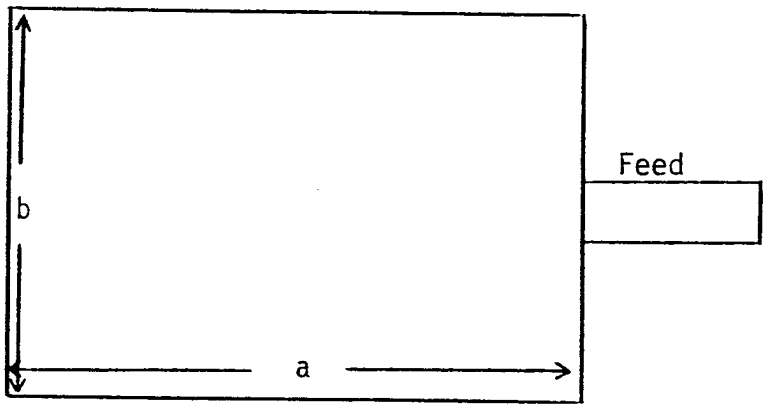

Figure 2.5 Rectangular microstrip antenna with the feed located at the radiating edges.

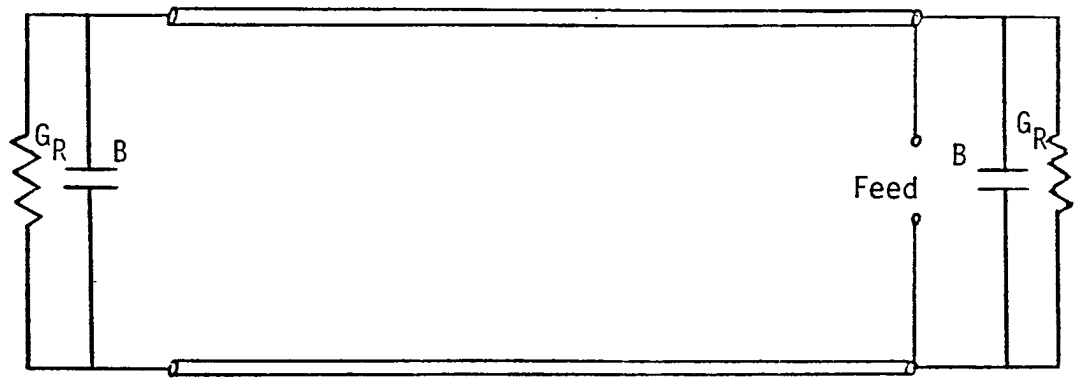

Figure 2.6 Equivalent transmission line model of the rectangular microstrip antenna fed at the radiating edge.

Even though (2.15) was derived to account for the probe effect in a coaxial type of feed, it is found to give an approximation to the reactances associated with a microstrip feed. Using (2.12)-(2.15), the input impedance seen at the microstrip feed is:

$$z_{in} = z_1 + jx_L \tag{2.16}$$

where $z_1 = 1/y_1$. (2.17)

Example: As an example of the use of this model, a rectangular antenna with the following parameters is considered:

frequency: $f = 7.5$ GHz

dielectric constant: $\epsilon_r = 2.48$

dielectric loss tangent: $\delta = 0.002$

substrate thickness: $h = 1/32$ in.

strip thickness: $t = 0.7$ mil

antenna width: $b = 1.5875$ cm

An optimization analysis is used to select antenna length a and feed location x_1 so as to make the input impedance z_{in} equal to that of the feed line ($z_0 = 50$). The pattern search optimization method of Hooke et al. [14] was used for this purpose. The optimum length a and the feed location x_1 thus obtained are:

antenna length: $a = 1.166$ cm

feed location: $x_1 = 0.3255$ cm

The computed input impedance using formulas (2.12) through (2.16) is found to be $z_{in} = 50.3 + j\ 0.2(\Omega)$. The corresponding

reflection coefficient at the feed plane is $|S_{11}| = 0.0025$.

2.5 Two-Port Transmission Line Model

The two port microstrip rectangular antenna shown in Fig. 2.7 is used as an element of a series feed array. This antenna can be analyzed using the transmission line model. The effects of radiation and fringing fields are incorporated into this model in the same way as was done for a single feed antenna. The equivalent transmission line model for this configuration is shown in Fig. 2.8.

First step in the analysis of the two port circuit of Fig. 2.8 is to transform the edge admittances to the locations (x_1, x_2) of external ports. Let y_o denote the characteristic admittance of the equivalent transmission line and y_{o1}, y_{o2} denote those of the transmission lines connected to the rectangular antenna. An equivalent circuit of that of Fig. 2.8 is shown in Fig. 2.9, where y_{L1}, y_{L2} are given by:

$$y_{L1} = y_o \frac{y_L \cosh(\gamma x_1) + y_o \sinh(\gamma x_1)}{y_o \cosh(\gamma x_1) + y_L \sinh(\gamma x_1)} \tag{2.18}$$

$$y_{L2} = y_o \frac{y_L \cosh(\gamma(a-x_2)) + y_o \sinh(\gamma(a-x_2))}{y_o \cosh(\gamma(a-x_2)) + y_L \sinh(\gamma(a-x_2))} \tag{2.19}$$

x_L accounts for the effects of the parasitic reactances at the feed point and is given by (2.15).

The analysis of the circuit is carried out in terms of the A matrices. The circuit of Fig. 2.9 is subdivided into three cascaded elements as shown.

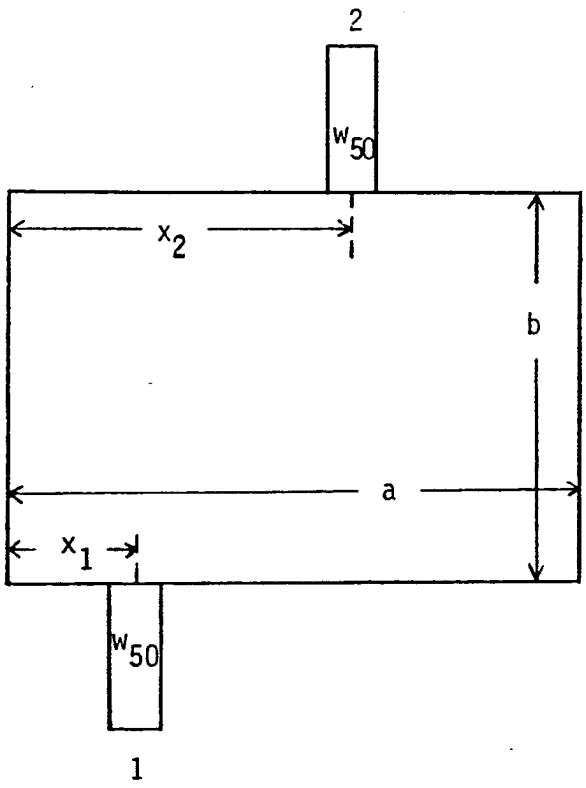

Figure 2.7 A two-port rectangular microstrip patch antenna.

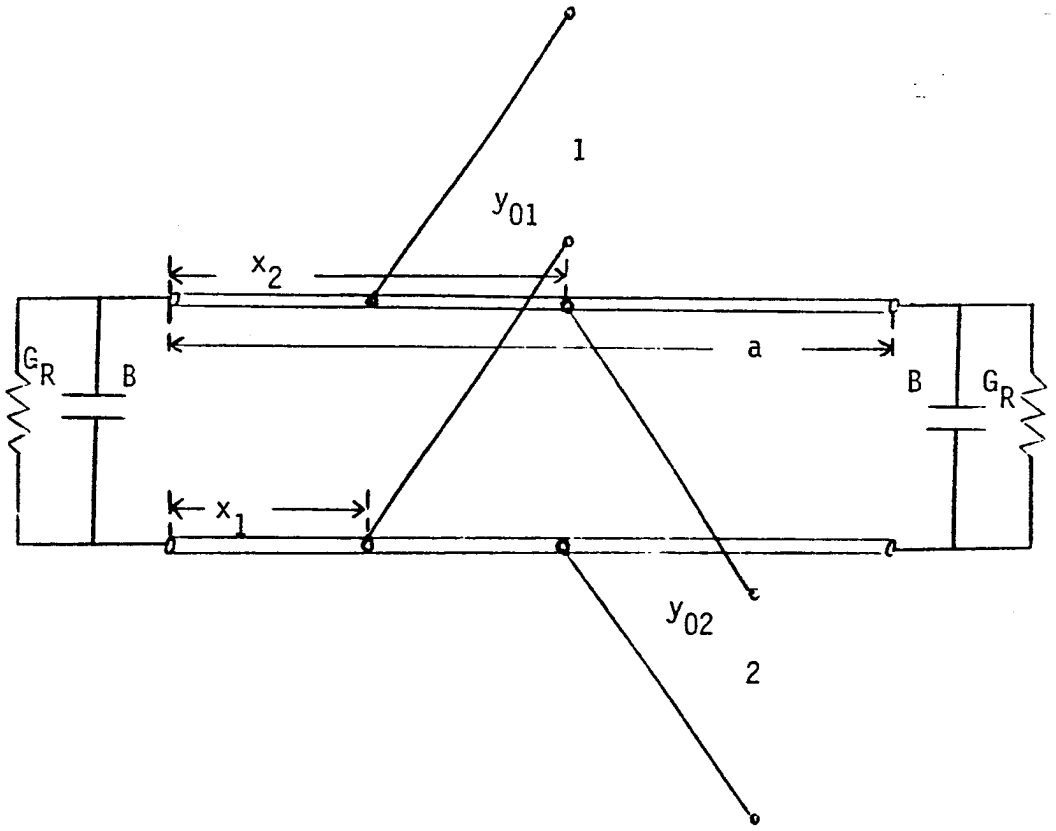

Figure 2.8 Equivalent transmission line of a two-port rectangular microstrip antenna.

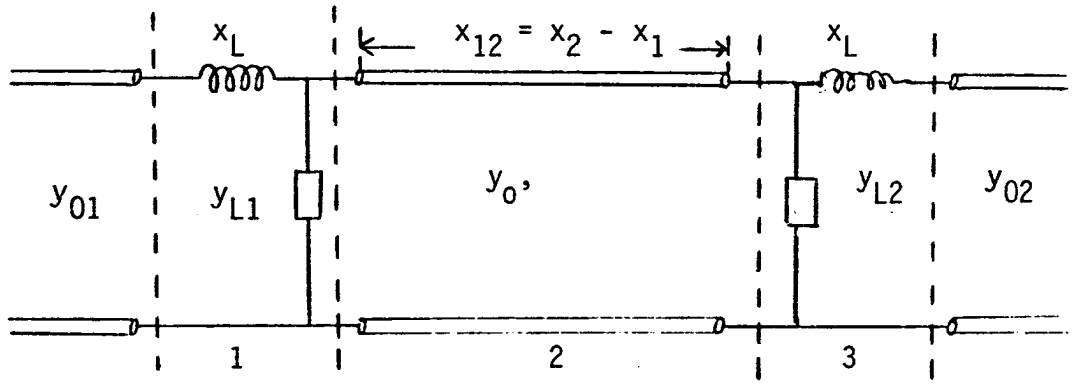

Figure 2.9 Multiport network representation of the equivalent transmission line model.

The A matrix for the first element which is a series inductance and a shunt admittance, is given by:

$$|A_1| = \begin{bmatrix} 1 + jx_L y_{L1} & jx_L \\ y_{L1} & 1 \end{bmatrix} \tag{2.20}$$

The A matrix for the second element, which is a section of the transmission line of characteristic impedance z_o and length $x_{12} = x_2 - x_1$ is:

$$|A_2| = \begin{bmatrix} \cosh(\gamma x_{12}) & \dfrac{\sinh(\gamma x_{12})}{y_o} \\ y_o \sinh(\gamma x_{12}) & \cosh(\gamma x_{12}) \end{bmatrix} \tag{2.21}$$

Finally, the A matrix for the third element is:

$$|A_3| = \begin{bmatrix} 1 & jx_L \\ y_{L2} & 1 + jx_L y_{L2} \end{bmatrix} \tag{2.22}$$

The overall matrix for the two-port network is then given by

$$|A| = |A_1| \cdot |A_2| \cdot |A_3| \tag{2.23}$$

$$|A| = \begin{bmatrix} A_{11} & A_{12} \\ A_{21} & A_{22} \end{bmatrix} \tag{2.24}$$

The elements of the matrix A in (2.24) are computed by carrying out the matrix multiplication in (2.24)

The element of the matrix S for the two-port network of Fig. 2.9 are related to those of the A matrix as follows [4].

$$S_{11} = (A_{11}Z_{02} + A_{12} - A_{21}Z_{01}Z_{02} - A_{22}Z_{01})/E \tag{2.25a}$$

$$S_{12} = S_{21} = 2\sqrt{Z_{01}Z_{02}}\ /E \tag{2.25b}$$

$$S_{22} = (-A_{11}Z_{02}+A_{12}-A_{21}Z_{01}Z_{02}+A_{22}Z_{01})/E \tag{2.25c}$$

where

$$E = A_{11}Z_{02} + A_{12} + A_{21}Z_{01}Z_{02} + A_{22}Z_{01} \tag{2.25d}$$

The elements of the Z matrix are related to those of the A matrix as follows:

$$Z_{11} = A_{11}/A_{21} \tag{2.26a}$$

$$Z_{21} = z_{12} = 1/A_{21} \tag{2.26b}$$

$$Z_{22} = A_{22}/A_{21} \tag{2.26c}$$

For some applications of two-port microstrip antennas it is desired to compute the input impedance at one port when the second port is matched. In this case the current and voltage at the second port are related by:

$$V_2 = - Z_{02}I_2 \tag{2.27}$$

Using (2.26) and (2.27) the input impedance can be shown to be:

$$Z_{in} = Z_{11} - \frac{Z_{12}^2}{Z_{11}+Z_{02}} \tag{2.28}$$

where Z_{02} is the characteristic impedance of the transmission line connected to the second port.

Example. The application of the two-port transmission model discussed in this section is illustrated in the following example. It is required to find the antenna parameters such that a match between the feed line and the antenna is accomplished when the second port is terminated on its characteristic impedance ($Z_{02} = Z_{01} = 50\ \Omega$). The antenna parameters design are:

frequency: $f = 7.5$ GHz

dielectric constant: $\varepsilon_r = 2.48$

substrate thickness: $h = 1/32$ in.

antenna width: $b = 1.5875$ cm

input port location: $x_1 = 0.3$ cm

The remaining design parameters were found using an optimization program and are found to be as:

location of the second port: $x_2 = 0.476$ cm

antenna resonant length: $a = 1.172345$ cm

The calculated input impedance is:

$$Z_{in} = 49.62 + j\ .15\ (\Omega)$$

Summary. We presented in this chapter the available formulation for the edge admittance. Then we discussed the

application of transmission line model to the analysis of the rectangular patch operating in the TM_{10} mode. The effects of the feed reactances are approximated by a series inductance, derived for a coaxial feed. This assumption gives good agreement with the two-dimensional analysis discussed in the next chapter.

CHAPTER III

TWO-DIMENSIONAL ANALYSIS OF RECTANGULAR MICROSTRIP ANTENNAS

3.1 Introduction

Since the heights of substrates used are much smaller than the wavelength, there is no variation of fields in the z-direction (Fig. 3.1) except at the edges and the microstrip patch antennas can be treated as two-dimensional structures. They can be analyzed and designed using a two-dimensional analysis [15].

The segmentation method is one of the methods used for the analysis of two-dimensional structures. In this method, the antenna is modelled as a multiport network. The antenna configuration is divided into segments which are characterized by their impedance matrices. The impedance matrices for the various segments are combined to find the overall impedance matrix of the multiport network which models the antenna. In the first section a derivation of the Z-matrix for a rectangular planar component is presented. Then application of the segmentation method to two configurations with one and two port rectangular microstrip antennas is discussed.

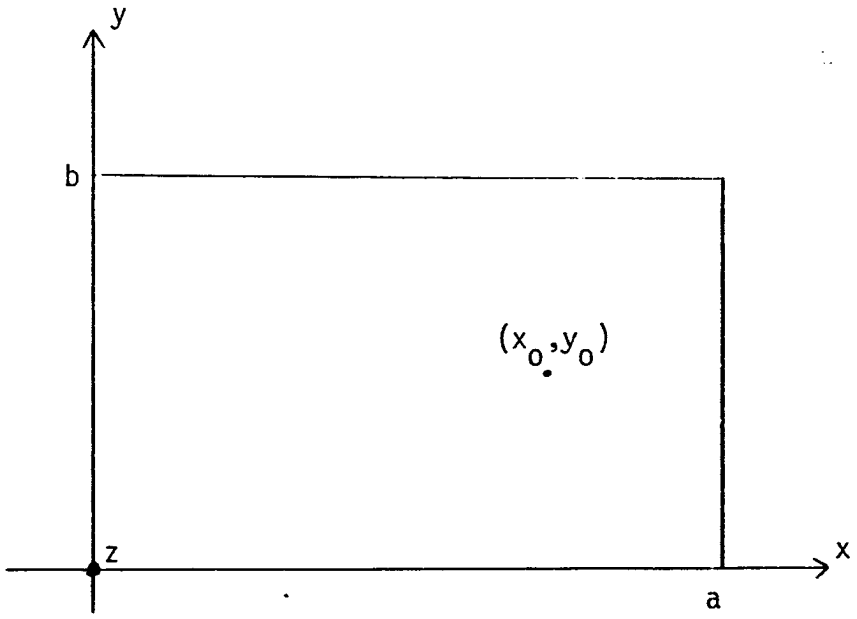

Figure 3.1 A rectangular planar component with feed location.

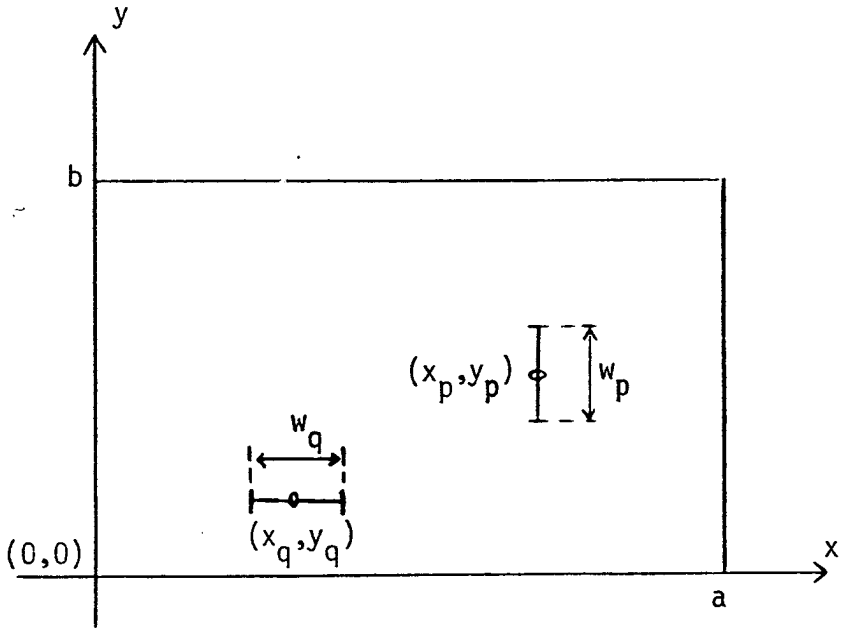

Figure 3.2 A rectangular planar component showing the width and orientation of port p and q.

3.2 Z-Matrix of a Rectangular Planar Component

In this section the impedance matrix of a multiport rectangular planar component is derived. The available formulation is to be compared with a new formulation. The two formulations are based on the Green's function approach.

3.2.1 Green function and available formulation

Consider a rectangular planar component with dimensions a and b filled with a dielectric material having constant μ_0, ε. Assuming no field variation along the z-direction, the only field components present are the z-component of the electric field and x and y components of the magnetic field. The E_z component satisfies the two-dimensional Helmholtz equation which may be written as:

$$(\nabla_T^2 + k^2)E_z(x,y) = 0, \quad \nabla_T^2 = \frac{\partial^2}{\partial x^2} + \frac{\partial^2}{\partial y^2} \tag{3.1}$$

A voltage can be defined for two-dimensional components as:

$$V(x,y) = h \cdot E_z(x,y) \tag{3.2}$$

This voltage can be related to the excitation source current $i(x_0,y_0)$ by an impedance Green function defined by:

$$V(x,y) = \iint G(x,y|x_0,y_0) \cdot i(x_0,y_0) dx_0 dy_0 \tag{3.3}$$

where $G(x,y|x_0,y_0)$ is a solution of

$$(\nabla_T^2 + K^2)G = -j\omega\mu h\delta(\bar{r}-\bar{r}_0) \tag{3.4}$$

$\bar{r}$ denotes the voltage point and $\bar{r}_o$ refers to the source location. An equivalent fictitious z-directed current density for a port on the periphery may be written as [3]

$$J_s = \frac{-1}{j\omega\mu d} \frac{\partial V}{\partial n} \bar{a}_z \tag{3.5}$$

where n is the outward normal to the periphery. The current i_p fed at the pth port of width w_p as shown in Fig. 3.2 is:

$$i_p = - \int_{w_p} J_s(x_o,y_o)dr_o \tag{3.6}$$

using (3.4) and (3.7) and assuming the voltage and the current density are constant over w_p and w_q, an alement of the z-matrix is given by

$$z_{pq} = \frac{1}{w_p w_q} \int_{w_p} \int_{w_q} G(x_p,y_p|x_q,y_q)dr_p dr_q \tag{3.7}$$

where dr_p, dr_q are incremental distances over the port width w_p, w_q. Green's function $G(x_p,y_p|y_q,y_q)$ for a rectangular geometry with magnetic walls may be shown to be as [11].

$$G(x_p,y_p|x_q,y_q) = \frac{j\omega\mu d}{ab} \sum_{n=0}^{\infty} \sum_{m=0}^{\infty} \sigma_m \sigma_n \frac{\cos(k_x x_p)\cos(k_y y_p)\cos(k_x x_q)\cos(k_y y_q)}{k_x^2 + k_y^2 - k^2} \tag{3.8}$$

where $k_x = \frac{m\pi}{a}$, $k_y = \frac{n\pi}{b}$

$$\sigma_m = \begin{cases} 1, & m = 0 \\ 2, & m \neq 0 \end{cases}$$

$k^2 = \omega^2 \mu_o \varepsilon_o \varepsilon_r (1-j\delta)$, δ is the loss tangent of the dielectric.

For a rectangular planar circuit fed by microstrip line, all ports are oriented along the edges. When the coordinate axes are along the sides of the rectangle (as shown in Fig. 3.2), it follows that those ports are oriented either along the x-direction or the y-direction. This yields the following expression for the elements of the Z-matrix for the rectangular component:

$$Z_{qp} = \frac{j\omega\mu d}{ab} \sum_{m=0}^{\infty} \sum_{n=0}^{\infty} \phi_{mn}(x_p,y_p)\phi_{mn}(x_q,y_q)(k_x^2 + k_y^2 - k^2)^{-1} \quad (3.9)$$

where for ports oriented along the y-direction and having a width w:

$$\phi_{mn}(x,y) = \cos(k_x x)\cos(k_y y)\mathrm{sinc}(\frac{k_y w}{2}) \quad (3.10)$$

and for ports oriented along the x-direction:

$$\phi_{mn}(x,y) = \cos(k_x x)\cos(k_y y)\mathrm{sinc}(\frac{k_x w}{2}) \quad (3.11)$$

where

$$\mathrm{sinc}(z) = \frac{\sin(z)}{z}$$

Expression (3.9) for Z_{pq} involves a doubly infinite series which is very slowly convergent. A method developed for increasing the convergence of this series representation is presented in the next section.

3.2.2 Improved formulation for the z-matrix

The proposed method consists of analytically carrying out the inner summation of (3.8). The details of the derivation are

given in Appendix A. From Appendix A, the new formulation for Green's function is given by

$$G(x_p,y_p|x_q,y_q) =$$

$$- CF \sum_{\ell=0}^{\infty} \sigma_\ell \cos(k_u u_p)\cos(k_u u_q) \frac{\cos(\gamma_\ell Z_>)\cos(\gamma_\ell Z_<)}{\gamma_\ell \sin(\gamma_\ell F)} \qquad (3.12)$$

where

$$F = \begin{cases} b, & \ell = m \\ a, & \ell = n \end{cases}, \quad (u_p,u_q) = \begin{cases} (x_p,x_q), & \ell = m \\ (y_p,y_q), & \ell = n \end{cases}$$

$$\gamma_\ell = \pm\sqrt{k^2-k_u^2}$$

and $k_u = \begin{cases} \frac{m\pi}{a}, & \ell = m \\ \frac{n\pi}{b}, & \ell = n \end{cases}$, $C = \frac{j\omega\mu d}{ab}$

and $(Z_>,Z_<) = \begin{cases} (y_>-b,\ y_<), & \ell = m \\ (x_>-a,\ x_<), & \ell = n \end{cases}$

where $y_{\substack{> \\ <}} = \begin{matrix}\max \\ \min\end{matrix} (y_p,y_q)$

The sign of γ_ℓ is chosen such that the imaginary part of γ_ℓ is negative.

a) Formulation for elements of the z-matrix.

Depending on the relative orientation and location of ports p and q, two cases are considered.

Case I: When both ports (p and q) are oriented along the same direction (x or y).

When the two ports are oriented along the y-direction, the integrations in (3.7) are with respect to the variable y(dr_p = dy and dr_q = dy). For the integration to be independent

of $Z_>$ and $Z_<$, the dummy variable ℓ is made equal to n, so $Z_> = x_>-a$ and $Z_< = x_<$. But when the two ports are oriented along the x direction, ℓ is made equal to m. These choices ensure the convergence of the series for Z_{pq}. Using (3.7) and (3.12), it can be shown that:

$$Z_{pq} = -CF \sum_{\ell=0}^{\infty} \sigma_\ell \cos(k_u u_p)\cos(k_u u_q)\cos(\gamma_\ell Z_>)\cos(\gamma_\ell Z_<) \cdot \frac{\operatorname{sinc}(\frac{k_u w_p}{2})\operatorname{sinc}(\frac{k_u w_q}{2})}{\gamma_\ell \sin(\gamma_\ell F)} \tag{3.13}$$

when ℓ becomes large, the imaginary part of the arguments of the complex trigonometric functions $\sin(\gamma_\ell F)$, $\cos(\gamma_\ell Z_<)$ and $\cos(\gamma_\ell Z_<)$ can become very large and will give rise to a numerical problem. To overcome this problem, the trigonometric functions are replaced by their large argument approximation as:

$$\begin{aligned} \cos(\gamma_\ell Z_>) &= \tfrac{1}{2} \exp(-j\gamma_\ell Z_>) \\ \cos(\gamma_\ell Z_<) &= \tfrac{1}{2} \exp(j\gamma_\ell Z_<) \\ \sin(\gamma_\ell F) &= \tfrac{1}{2j} \exp(j\gamma_\ell F) \end{aligned} \tag{3.14}$$

Using (3.13) and (3.14) the series expression for Z_{pq} may now be rewritten as:

$$\begin{aligned} Z_{pq} = -CF \sum_{\ell=0}^{L} \sigma_\ell \cos(k_u u_p)\cos(k_u u_q)\cos(\gamma_\ell Z_>)\cos(\gamma_\ell Z_<) \\ \cdot \frac{\operatorname{sinc}(\frac{k_u w_p}{2})\operatorname{sinc}(\frac{k_u w_q}{2})}{\gamma_\ell \sin(\gamma_\ell F)} - jCF \sum_{\ell=L+1}^{\infty} \cos(k_u u_p)\cos(k_u u_q) \\ \cdot \operatorname{sinc}(\frac{k_u w_p}{2})\operatorname{sinc}(\frac{k_u w_q}{2}) \frac{\exp(-j\gamma_\ell(v_>-v_<))}{\gamma_\ell} \end{aligned} \tag{3.15}$$

where

$$(v_>, v_<) = \begin{cases} (y_>, y_<), & \ell = m \\ (x_>, x_<), & \ell = n \end{cases}$$

The choice of L in (3.15) is a compromise between fast convergence and accuracy. Practically L is chosen such that $\gamma_\ell F$ is greater than or equal to 500.

Case II: When the two ports (p and q) are oriented in different directions x and y.

For this case, Z_{pq} may be written as:

$$Z_{pq} = -CF \sum_{\ell=0}^{\infty} \sigma_\ell \cos(k_u u_p)\cos(k_u u_q)\cos(\gamma_\ell Z_>)\cos(\gamma_\ell Z_<) \frac{\operatorname{sinc}(\frac{k_u w_i}{2})\operatorname{sinc}(\frac{\gamma_\ell w_j}{2})}{\gamma_\ell \sin(\gamma_\ell F)} \tag{3.16}$$

When $\ell = n$, w_i corresponds to the port oriented along the y-direction and w_j corresponds to the port along the x-direction. On the other hand if $\ell = m$, w_i is for the port along the x-direction and w_j for the port along the y-direction. Making use of large argument approximations for complex trigonometric functions (3.14), Z_{pq} may be written as:

$$Z_{pq} = -CF \sum_{\ell=0}^{L} \sigma_\ell \cos(k_u u_p)\cos(k_u u_q)\cos(\gamma_\ell Z_>)\cos(\gamma_\ell Z_<) \cdot \frac{\operatorname{sinc}(\frac{k_u w_i}{2})\operatorname{sinc}(\frac{\gamma_\ell w_j}{2})}{\gamma_\ell \sin(\gamma_\ell F)} - \frac{1}{2} CF \sum_{\ell=L+1}^{\infty} \sigma_\ell \cos(k_u u_p)\cos(k_u u_q) \cdot \operatorname{sinc}(\frac{k_u w_i}{2}) \frac{\exp(-j\gamma_\ell(v_> - v_< - w_j/2))}{\gamma_\ell^2 \cdot w_j} \tag{3.17}$$

The choice of the dummy variable ℓ is made by nothing that for the fast convergence of the summation (3.17) it is required that

$$(v_> - v_< - \frac{w_j}{2}) > 0 \tag{3.18}$$

3.2.3 Comparison of the two formulations

A comparison of the available formulation with the new formulation is made by considering a rectangle with dimensions $3\lambda/8 \times 3\lambda/8$ at a frequency $f = 3.$ GHz as shown in the inset of Fig. (3.3) where

$$\lambda = \frac{3.10^8}{\sqrt{\varepsilon_r}\, f} \text{ (m)} \tag{3.19}$$

A substrate having a thickness $h = 1/32$ in., $\varepsilon_r = 2.53$ and a nominal loss tangent of 0.001 have been considered. The input impedance of this rectangle (Fig. 3.3) at the location shown ($x = 0$, $y = \lambda/8$), using both formulations, is computed. The percentage error in the input impedance versus the time of computation in CPU-seconds is shown in Fig. 3.3. This figure shows the appreciable computational efficiency offered by the new series formulation. Numbers in parentheses along the two curves indicate the number of terms in the summation at that stage. For instance, to get an error in Z_{in} less than or equal to 1.%, 10 terms or less are needed for the new formulation. Whereas, at least (200×200) terms are required for the doubly infinite series. The computation times are respectively 0.2 and 80 CPU seconds.

For all practical numerical computations, 100 terms for the new method will assure good accuracy.

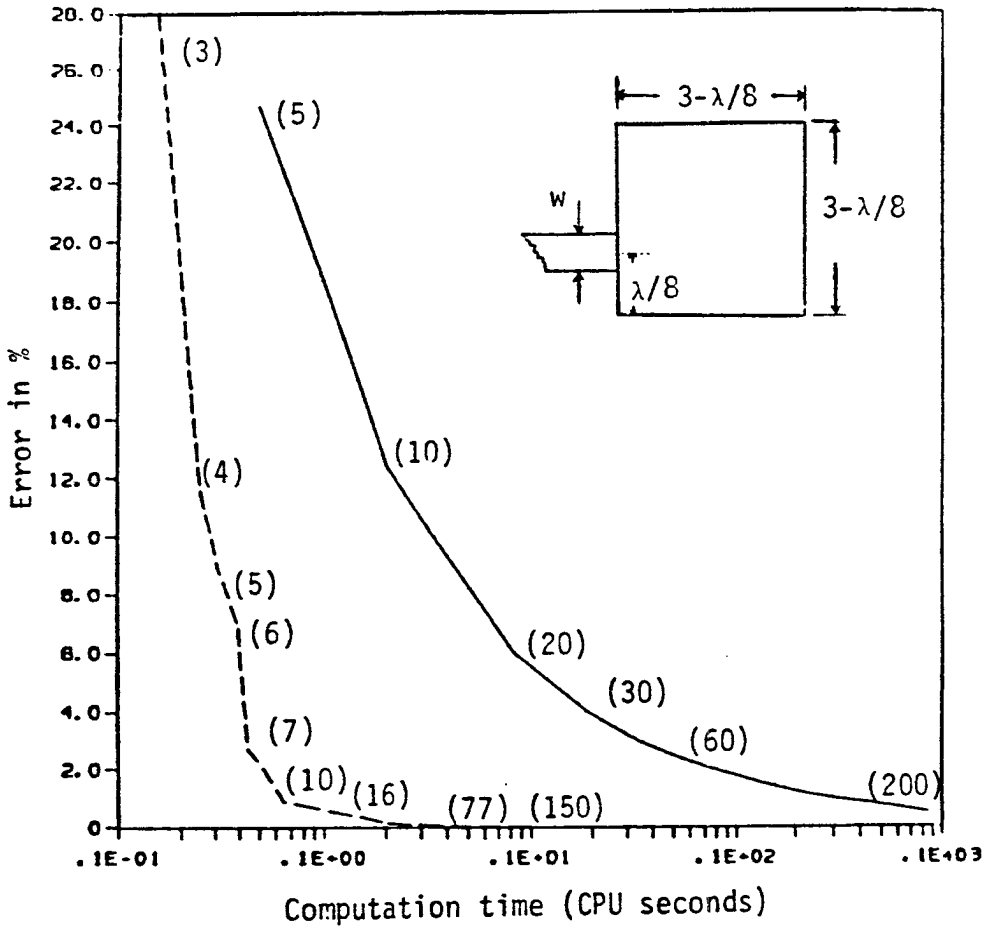

Figure 3.3 Comparison of the two series formulations for the computation of elements of the Z-matrix.

3.3 Edge Admittance Matrix

The edge admittance matrix y_E represents the effects of radiation, surface waves and fringing fields from both edges of the rectangular microstrip antenna shown in Fig. 2.1. Each edge of effective width b_e is divided into small sections as shown in Fig. 3.4. The number of sections is chosen such that the fields are constant over each section. These sections are considered as ports of a multiport network modelling the edge admittance. Each section is terminated in a load equal to the total edge-admittance (chapter II) divided by the total number of ports at one edge [5]. If N_C denotes the total number of ports at both edges, the y_E will be an $(N_C \times N_C)$ matrix having all entries equal to zero except those of the principal diagonal and can be expressed as:

$$[y_E] = 2\cdot(G_R + jB)/N_C\cdot\underset{\sim}{I} \tag{3.20}$$

$\underset{\sim}{I}$ is the identity matrix and G_R and B are given in chapter II.

3.4 Segmentation Method

The mathematical formulation of the segmentation technique is illustrated here by combining two multiports subnetworks, as shown in Fig. 3.5, to yield an overall multiport network as shown in Fig. 3.6. It is assumed that the two impedance matrices of the two subnetworks, denoted by $[Z_A]$ and $[Z_B]$ are known.

A reduction in computational effort is achieved if the connected ports (denoted by q for subnetwork A and by r for subnetwork B) are suitably regrouped 13 . This is done in such

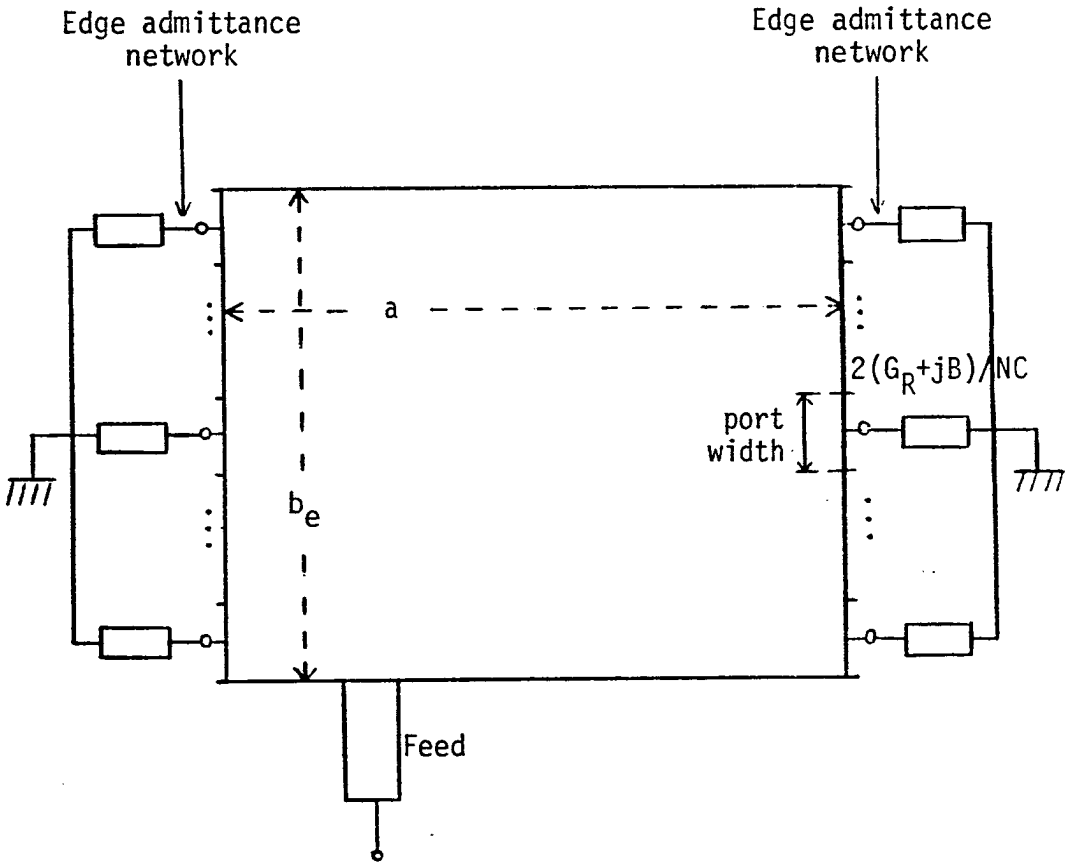

Figure 3.4 Multiport network representation of the edge-admittance segment.

a way that q_1 and r_1 ports are connected together, q_2 and r_2 are connected together and so on. The external ports for each subnetwork (denoted by p_1 for A and p_2 for B) are numbered first. Then the z-matrices for the two subnetworks can be written together as:

$$\begin{bmatrix} v_p \\ v_q \\ v_r \end{bmatrix} = \begin{bmatrix} Z_{pp} & Z_{pq} & Z_{pr} \\ Z_{qp} & Z_{qq} & Z_{qr} \\ Z_{rp} & Z_{rq} & Z_{rr} \end{bmatrix} \begin{bmatrix} I_p \\ I_q \\ I_r \end{bmatrix} \tag{3.21}$$

where $p = p_1 + p_2$, $q = r$ and where v_p and I_p are the voltage and current variables at the p external ports, and v_c and I_c are the corresponding variables at the internal ports. The interconnection constraints, that the voltages at two connected ports be equal and the sum of currents at the two connected ports be zero, can be expressed as:

$$v_q = v_r \tag{3.22}$$

and

$$I_q + I_r = 0$$

Substituting relations (3.22) into (3.21) and eliminating v_q and I_r we obtain the Z-matrix for the overall network shown in Fig. 3.7

$$Z_c = Z_{pp} + (Z_{pq}-Z_{pr})(Z_{qq}-Z_{qr}-Z_{rq}+Z_{rr})^{-1}\cdot(Z_{rp}-Z_{qp}) \tag{3.23}$$

Substituting also (3.22) into (3.21) and eliminating v_p and I_r, the voltages at the connected ports are related to the currents

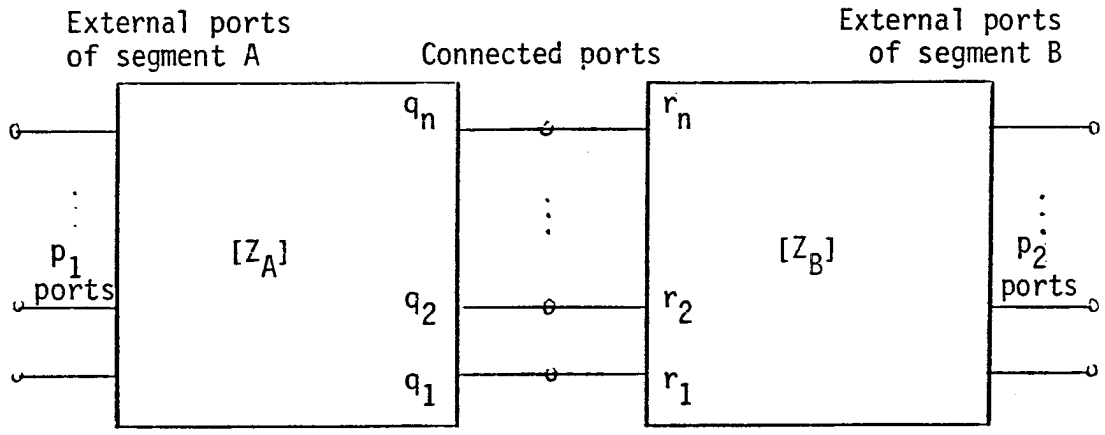

Figure 3.5 Two multiport network segments

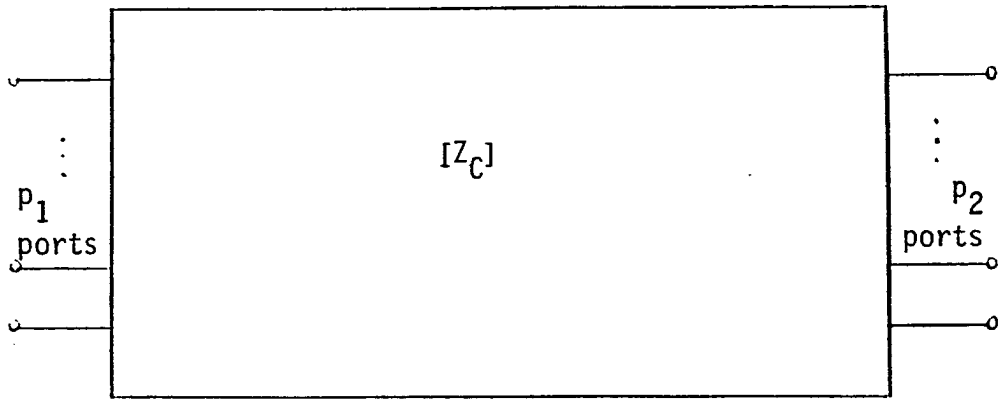

Figure 3.6 Overall multiport network segment.

flowing in the external ports p by:

$$v_q = \left[Z_{qp} + (Z_{qq}-Z_{qr})(Z_{qq}-Z_{qr}-Z_{rq}+Z_{rr})^{-1}\cdot(Z_{rp}-Z_{qp})\right] I_p \qquad (3.24)$$

Expression (3.23) and (3.24) will be used for the analysis of single feed and two-port rectangular microstrip antennas in subsequent sections.

3.5.1 Application of the segmentation method to single feed antennas

The rectangular microstrip antenna shown in Fig. 2.1 can be analyzed using the segmentation method. For this purpose, the rectangular antenna is modelled as a multiport network, which can be viewed as the combination of three multiport subnetworks as illustrated in Fig. 3.7.

Segment A is a multiport rectangular resonator with dimensions a and b_e. The effective width b_e is introduced in place of the physical width b to account for the effects of fringing fields at the non-radiating edges. Also we use an effective dielectric constant ε_{re} to account for the fields being partially in the substrate and partially in air. The impedance matrix Z_A of this segment is derived using the Z-matrix of a rectangular planar component given in section 3.2. This is done by replacing b by b_e and ε_r by ε_{re}. The size of the matrix Z_A is $(N_C+N_D)\times(N_C+N_D)$. N_C denotes the number of connected ports at the radiating edges of width b_e, N_D denotes the number of connected ports at the feed discontinuity as shown in Fig. 3.7.

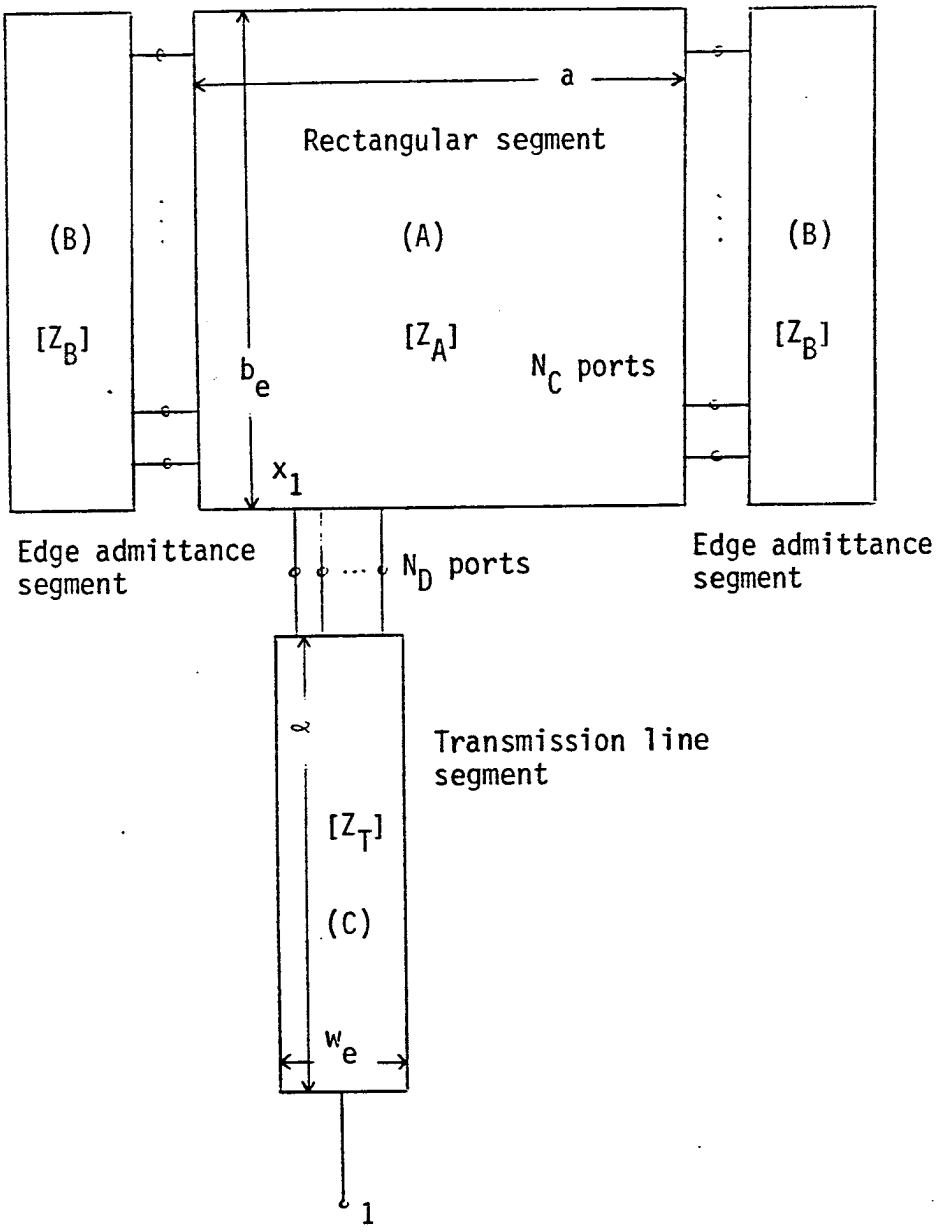

Figure 3.7 Multiport network representation of a single fed rectangular microstrip antenna.

Segment B represents the edge admittance at the two radiating edges and is characterized by the edge-impedance matrix Z_E, which is related to the edge-admittance matrix (given by 3.20) by:

$$[Z_E] = [y_E]^{-1} \tag{3.25}$$

or explicitly by:

$$[Z_E] = \frac{N_C}{2(G_R+jB)} \cdot \underset{\sim}{I} \tag{3.26}$$

The introduction of this segment is a means of separating the internal field of the patch from the external field of the microstrip antenna, permitting the use of magnetic wall boundaries at the radiating edges. The size of the matrix Z_E is $(N_C \times N_C)$.

Segment C represents the transmission line feed. The latter is considered as a planar rectangular component in order to account for the effects of any higher order evanescent modes that may be excited by the discontinuity at the feed location. The equivalent rectangular component of this segment has an effective width w_e and an effective dielectric constant ε_{re} corresponding to that of the microstrip feed line. The transmission line length ℓ is taken long enough to make the higher order evanescent modes decay out and leave only the TEM mode at the external port. The transmission line will be characterized by the impedance matrix z_T of size $(N_D+1)\times(N_D+1)$, which is derived using the results of section 3.2.

a) Combining transmission line segment with patch.

A good computational efficiency may be achieved by using partial segmentation. In this approach the three segments shown in Fig. 3.7 are segmented two at a time. In the first step, the transmission line segment is combined to the rectangular patch. The numbering of the ports for each segment is as shown in Fig. 3.8. The external ports are numbered first, then the connected ports are numbered as discussed in section 3.4. The resulting multiport is characterized by the impedance matrix Z_c. The numbering of ports for this network is as illustrated in Fig. 3.9.

b) Combining edge impedance segment.

The multiport network characterized by the impedance matrix Z_c is now combined with the edge impedance segment. The numbering of the ports of the edge impedance network is shown in Fig. 3.9. The application of the segmentation method yields directly the input impedance, as given by (3.23), and the voltages at the radiating edge, as given by (3.24).

3.5.2 Optimization procedure

One of the aims of analyzing the antenna of Fig. 2.1 is to find its parameters (width b, length a, feed location $x_1 \ldots$), so a match between the feed line and the patch is achieved. This is done in a systematic way by using an optimization procedure. One starts with a given set of parameters which are then iteratively modified until optimum parameters are reached. An optimization procedure based on the direct search method [14] is used for the design of one-port and two-port antennas.

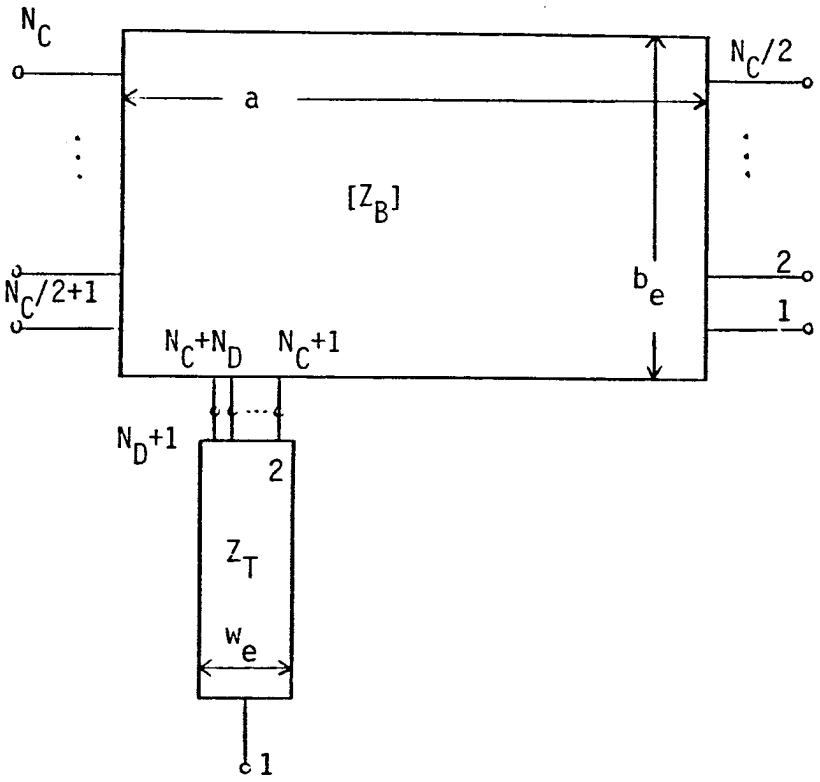

Figure 3.8 Numbering of the ports for combining the transmission line and rectangular segments

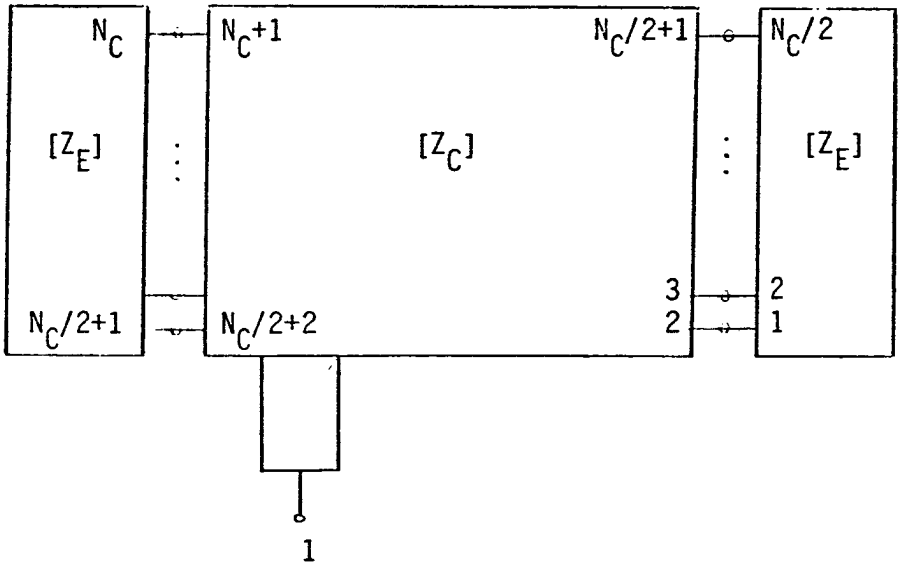

Figure 3.9 Numbering of the ports for combining the edge admittance network.

3.5.3 Feed location

In the present design, the antenna is fed by a microstrip line as shown in Fig. 2.1. The feed location is chosen to be along the non-radiating edge of the antenna. This choice leads to a wide range of values for the input impedance. This is due to the cosine type of variation of the voltage along the non-radiating edges when the antenna is operating in the dominant mode, TM_{10}.

a) Feed discontinuity effects.

Since the effective width of the feed is not negligible, the voltage is not constant along the interface between the feed and the patch. Therefore more than one port is needed at this interface. Table 3.1 shows the variation of the input impedance Z_{in} with the number of connected ports N_D at the discontinuity. It is seen from Table 3.1 that the value of Z_{in} converges with the increasing number of ports N_D. A value of N_D equal to 4 yields good accuracy ($\leq .8\%$).

The feed discontinuity has slight effects on the value of the voltages at the radiating edges. Table 3.2 shows an example of these effects on the average voltage for values of N_D from 1 to 7. These effects are accurately accounted for by making N_D equal to 4.

b) Transmission line length.

To assure that the higher order evanescent modes have decayed out and only the TEM mode is present at the external port, the transmission line length must be selected appropriately. The variation of the reflection coefficient magnitude along the

Table 3.1 Effects of Feed Discontinuity on the Input Impedance

# of ports N_D	Input impedance Z_m [Ω]
1	57.115 - j11.910
2	50.534 - j 0.968
3	49.528 - j .388
4	49.088 - j .145
5	48.871 - j .046
6	48.753 - j 0.008
7	48.675 - j 0.041

f = 7.5 GHz

ε_r = 2.48

h = 1/32 in.

δ = 0.002

feed length = 2.5 cm

w_e = 0.417 cm

b = 1.5875 cm

a = 1.17088 cm

x_1 = 0.31533 cm

N_C = 8

Table 3.2 Effects of Feed Discontinuity on the Average Voltage at the Radiating Edges

# of ports N_D	Voltage at the port #1
1	105.73
2	99.60
3	98.60
4	98.20
5	98.0
6	97.80
7	97.79

$f = 7.5$ GHz

$\varepsilon_r = 2.48$

$h = 1/32$ in.

$\delta = 0.002$

feed length = 2.5 cm

$w_e = 0.417$ cm

$b = 1.5875$ cm

$a = 1.17088$ cm

$x_1 = 0.31533$ cm

$N_C = 8$

transmission line length is plotted in Fig. 3.10. The reflection coefficient decreases by moving away from the feed junction up to a distance of $\lambda_0/16$, then it remains constant. This shows that higher order modes have been decaying and only the TEM mode is present at a distance greater than $\lambda_0/16$. We conclude that for the antenna parameters considered here the feed line segment must be at least $\lambda_0/16$ long.

3.5.4 Voltages at the radiating edges

The voltages at the radiating edges are needed for the computation of the radiation characteristics. The effects of the microstrip feed are to cause the asymmetrical distribution of the voltages at the radiating edges. When the patch is matched to the feed, the voltage at the radiating edges is not uniform. To observe these effects we need more than one port along each radiating edge. Table 3.3 shows the variation of the input impedance versus the number of ports N_C at both radiating edges. A value of N_C equal to 8 leads to a good accuracy of the input impedance ($\leq$ 1.%). This value is good at and near resonance. Far away from resonance more ports would be needed.

Figure 3.11 shows the voltage distribution along the edge width. A value of $N_C = 8$ is chosen, because those voltages are computed at resonance. From Fig. 3.11 we see that the voltage distribution is indeed not uniform.

3.5.5 Input impedance

The segmentation method and the optimization are used to get an input impedance which is equal to the characteristic

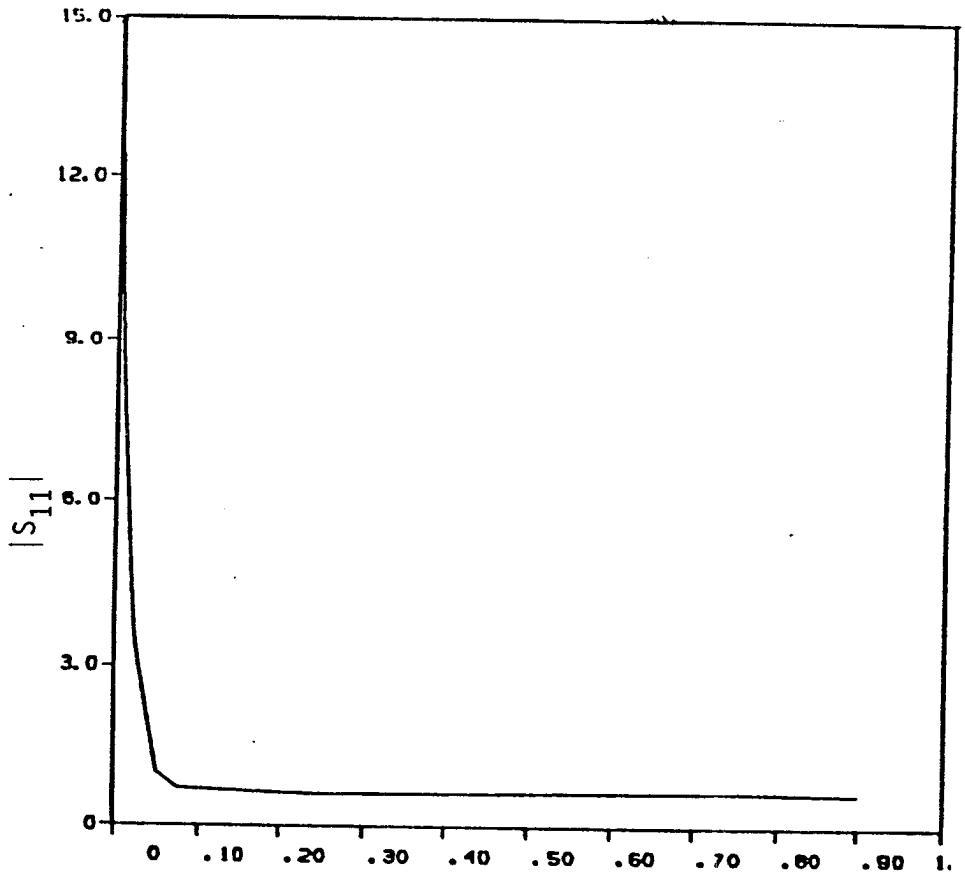

f = 7.5 GHz $\quad\quad$ ε_r = 2.48

a = 1.17088 cm $\quad\quad$ h = 1/32 in.

b = 1.5875 cm $\quad\quad$ x_1 = 0.31533 cm

Figure 3.10 Effects of feed discontinuity on the reflection coefficient along the transmission line length.

Table 3.3 Effects of Open End Discontinuity on the Input Impedance

# of ports N_C	Input impedance Z_{in} [Ω]
2	59.733 - j 1.729
4	52.296 - j 0.742
6	50.313 - j 0.489
8	49.527 - j 0.388
10	49.153 - j 0.336
12	48.94 - j 0.305
14	48.82 - j 0.285

f = 7.5 GHz

ε_r = 2.48

a = 1.17088 cm

feed length = 2.5 cm

b = 1.58750 cm

h = 0.79375 cm

x_1 = 0.31533 cm

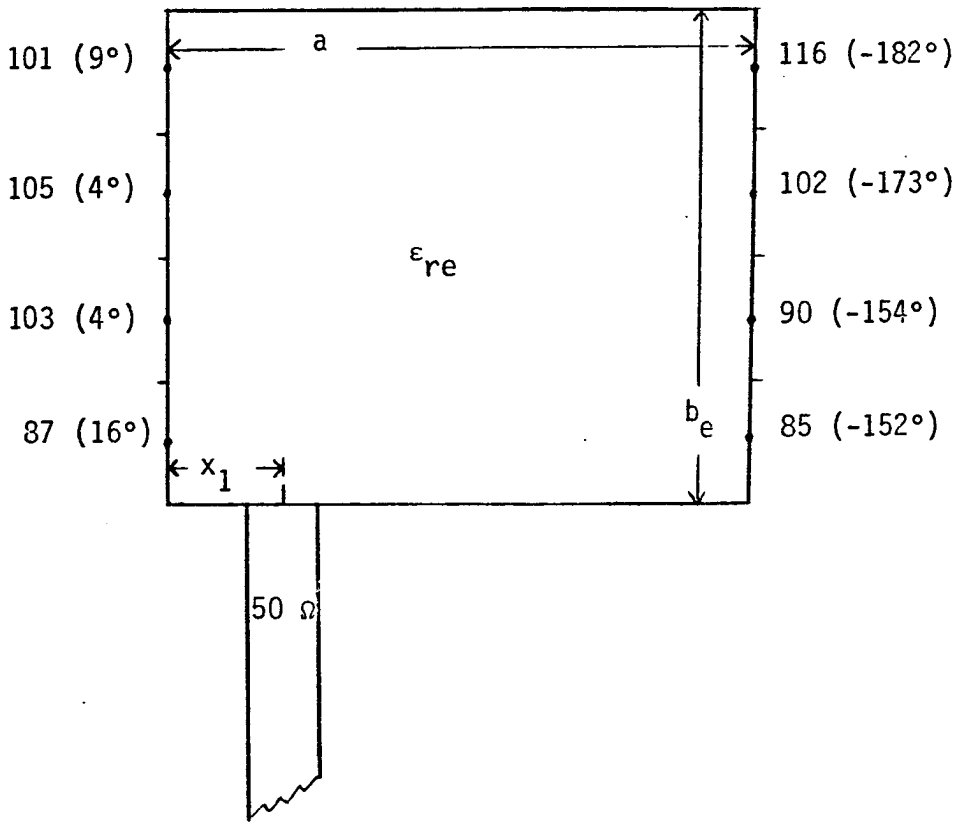

Figure 3.11 Voltage distribution at the radiating edges.

impedance of the feed line (Z_0 = 50). The computations are carried out using 4 ports at the feed discontinuity and 8 ports at the edges. The results of this analysis are compared to those using the transmission line model as shown in Table 3.4. The effects of feed reactance are accounted for in the transmission line model by using the approximate formula (2.15). It is noted that the results between the two models are in good agreement.

3.5.6 Bandwidth

The bandwidth of a microstrip antenna is usually limited by the input VSWR and is calculated by evaluating the input impedance as a function of frequency. Fig. 3.12 shows the input impedance locus on a Smith chart for an antenna whose parameters are given by:

antenna width: b = 1.5875 cm

antenna length: a = 1.17088 cm

frequency: f = 7.5 GHz

dielectric constant: ε_r = 2.48

substrate thickness: h = 1/32 in.

feed location: x_1 = 0.3153325 cm

The bandwidth of the antenna for a VSWR less than 2 is equal to 2.5%. This value for the bandwidth is typical for single feed antennas.

Table 3.4 Comparison of Single Feed Patch Designs Based on Segmentation Method and Transmission Line Model

	Segmentation method	Transmission line model	Difference
a (cm)	1.17088	1.1660	≈ 0.4%
x_1 (cm)	0.31533	0.32550	≈ 3.1%
Z_{in} (Ω)	49.5 - j 0.38	50.3 + j 0.2	≈ 1.6%

$f = 7.5$ GHz

$\varepsilon_r = 2.48$

$h = 1/32$ in.

$w_e = 0.417$ cm

$b = 1.5875$ cm

$Z_o = 10.5\ \Omega$

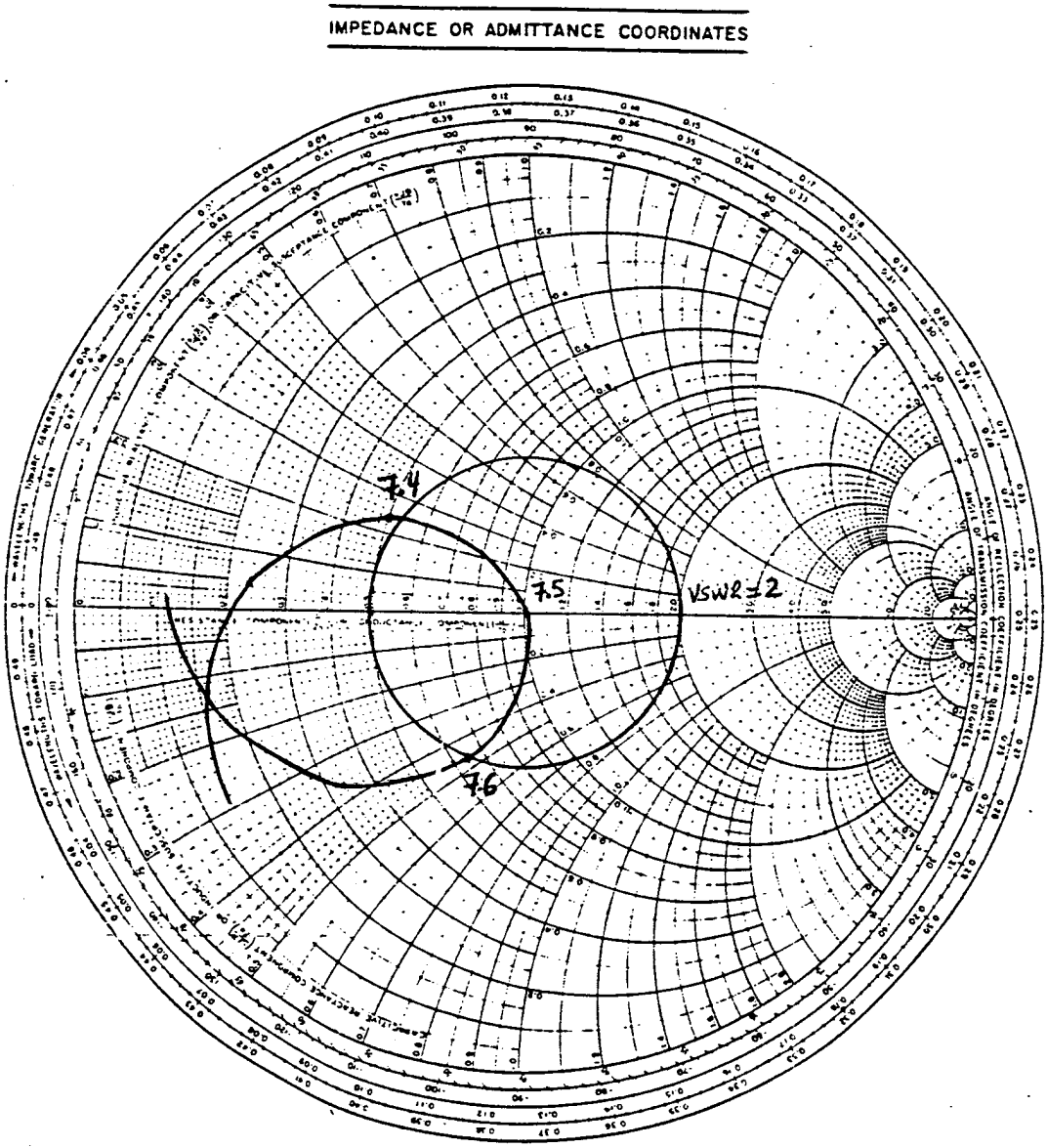

Figure 3.12 Impedance locus of a single fed rectangular microstrip antenna.

3.6 Two-Port Microstrip Antenna

The two-port rectangular microstrip antenna shown in Fig. 2.5, is commonly used as an element of a series feed array. This configuration can be analyzed using the segmentation method by dividing it into 4 multiport segments as shown in Fig. 3.13. Edge admittances at the two radiating edges constitute a single multiport network. The transmission lines are considered as planar components to account for the effects of junction reactances. The segmentation method is applied by combining two segments at a time. First, the rectangular patch is combined with the input transmission line network, then the resulting multiport network is combined to the output transmission line network. The edge-admittance network is combined last, in order to facilitate the computation of the voltages at the radiating edges.

In this section the segmentation method is used to calculate the characteristics (such as input impedance and bandwidth) of the two-port antennas. The results of this analysis are to be compared with those obtained using the transmission line model discussed in chapter II.

3.6.1 Input impedance

The input impedance of an antenna should be known in order to match the feed line to the patch antenna. As the location of the feed point along the non-radiating length can be varied it is possible to obtain the input match for a wide range of the antenna parameters. In fact, a given value of the input impedance can be

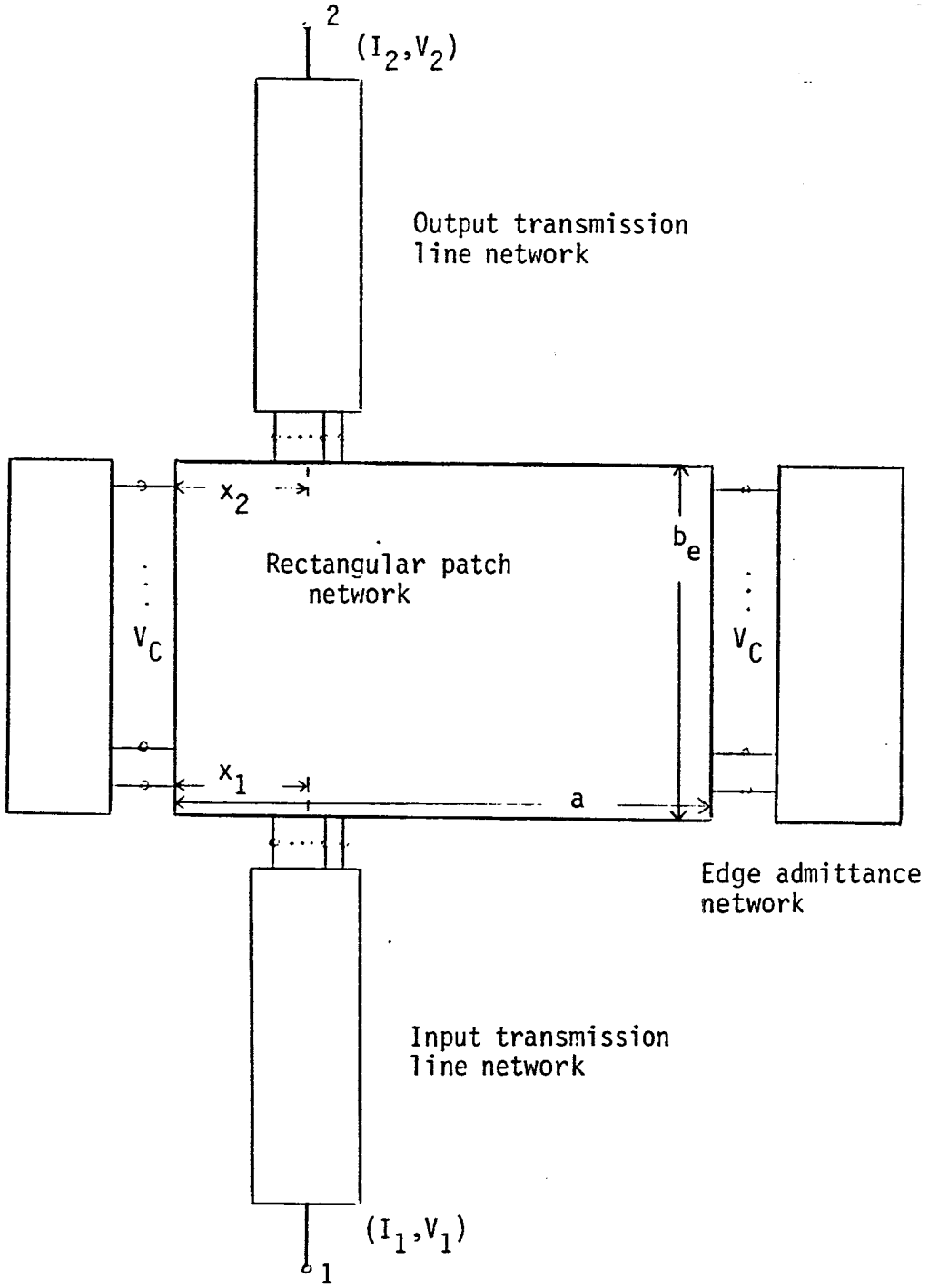

Figure 3.13 A multiport network representation of two-port rectangular microstrip antenna.

obtained for different relative locations of the two external ports and the antenna resonant length.

Comparison with the transmission line model.

Table 3.5 shows the input impedance computed using both the segmentation method and the transmission line model. Results of the transmission line model include, approximately, the effect of junction reactances as given by (2.15). The input impedance is computed by terminating the second port in its characteristic impedance ($Z_o = 50$), and taking $N_C = 8$ and $N_D = 4$. The results show an agreement between the two models.

3.6.2 Bandwidth

The bandwidth of the two-port antenna is calculated by plotting the input impedance versus frequency. Fig. 3.14 shows the impedance locus on a Smith chart as obtained from the segmentation method. The bandwidth is computed to be 2.7%, which is greater than that of a single feed antenna (which, as discussed earlier in section 3.5.6, is about 2.5%). Since the second port is matched, it loads the resonant structure and decreases the overall Q-factor.

3.6.3 Power transmitted to port 2

For an antenna array to have a specific side lobe level performance, the power distribution should be specified. The power transmitted to the second port can be controlled by varying either the relative locations of the two external ports or the antenna width. At resonance, when the feed line is matched to the

Table 3.5 Comparison of Two-Port Patch Designs Based on Segmentation Method and Transmission Line Model

	Segmentation method	Transmission line model	Difference in %
Z_{in} (Ω)	50.13 + j 0.96	49.62 + j .15	1.
a (cm)	1.18162	1.17234	0.7
x_2 (cm)	0.45527	0.47600	4.5

x_1 = 0.3 cm

f = 7.5 GHz

ε_r = 2.48

b = 1.5875 cm

h = 1/32 in.

tan δ = 0.002

t = 0.7 mil ($\frac{1}{2}$ oz copper)

Z_o = 10.5 Ω

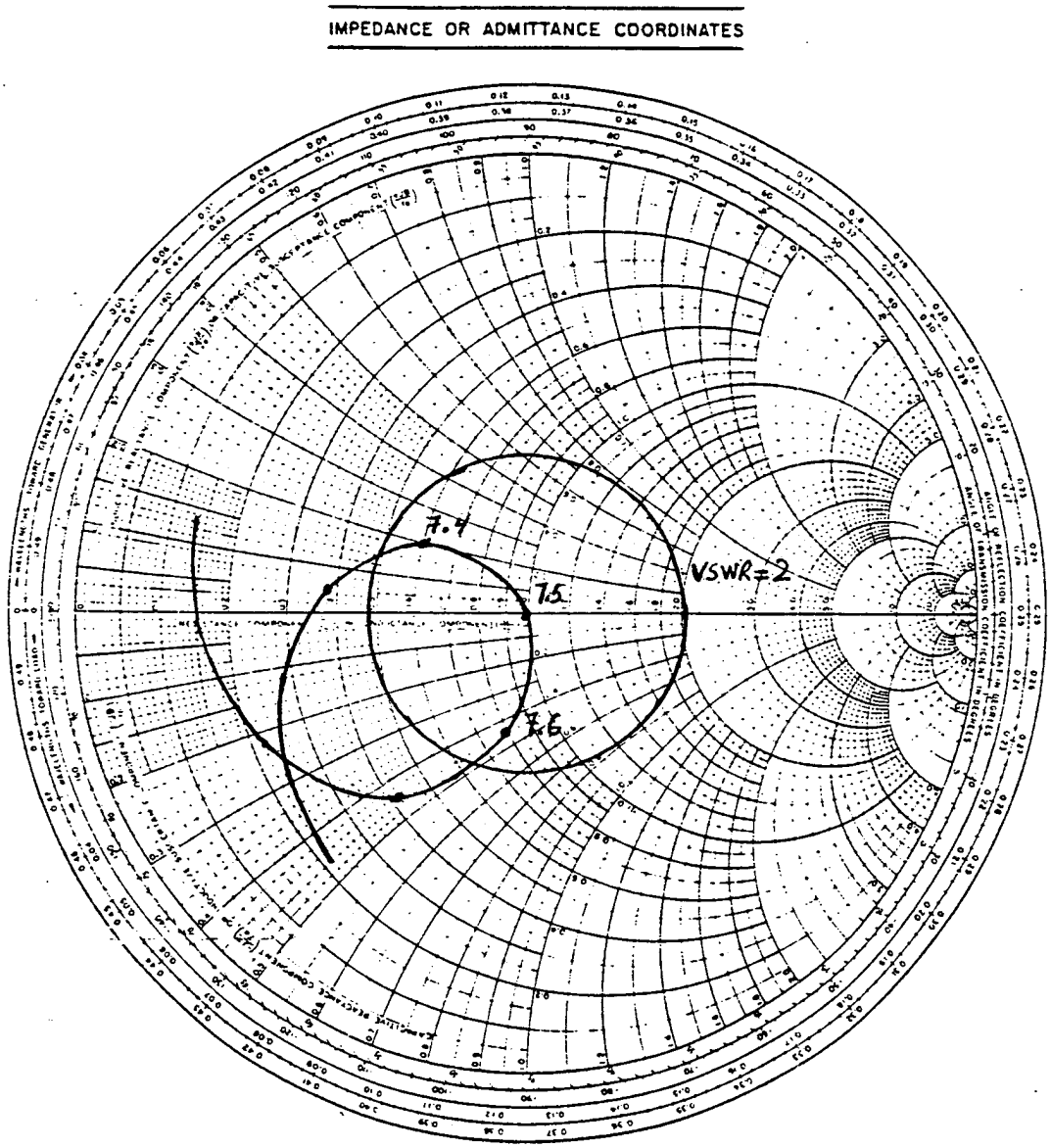

Figure 3.14 Impedance locus of a two-port rectangular microstrip antenna.

patch, the input power gets divided into the radiated power, the power transmitted to the second port and a part which is dissipated in dielectric and conductor losses.

When the second port is terminated in its characteristic impedance (which is the usual case in series feed arrays). The radiated power from the rectangular antenna is given by

$$P_{rad} = \frac{G_R}{N_C} \sum_{i=1}^{N_C} |V_C(i)|^2 \tag{3.27}$$

where N_C is the total number of ports taken at the two radiating edges, G_R is the radiation conductance associated with each edge as given in chapter II. $V_C(i)$ denotes various port voltages at the radiating edges, which is related to the currents flowing in the external ports (input feed and output line) by (3.24). Since port 2 is terminated in its characteristic impedance we have

$$I_2 = -V_2/Z_o$$

where V_2 and I_2 are the voltage and current variables at the external port 2 as shown in Fig. 3.13, Z_o is the characteristic impedance of both transmission lines. Using equations (3.23), (3.24), (3.27), (3.28) the radiated power from a unit applied voltage is:

$$P_{rad} = \frac{1}{4} \frac{G_R}{Z_o^2} \sum_{i=1}^{N_C} \left[Z_{Vi1} - \frac{Z_{Vi2} Z_{C12}}{Z_o + Z_{C22}}\right]^2 \cdot \frac{1}{NC} \tag{3.29}$$

Z_{vij} are the elements of the matrix Z_v defined by (3.24) as:

$$V_C = Z_V I_P \tag{3.30}$$

Z_{Cij} are the elements of the matrix Z_C defined by (3.23). The power transmitted to the second port per unit applied voltage is:

$$P_{trans} = \frac{1}{8Z_o}\left[\frac{Z_{C21}}{Z_o+Z_{C22}}\right]^2 \tag{3.31}$$

a) Variation of the transmitted power with the location of the external ports.

We have seen that an antenna match for a given input impedance can be achieved for different values of the relative locations of the external ports. Fig. 3.15 shows the locations x_1 and x_2 of the two ports for various percentages of transmitted power. This power is very small when the output port (port 2) is near the center (i.e., $x_2 \simeq a/2$) and increases when the feed is moved towards the corner. The resonant length a increases slightly when the feed is moved towards the corners. This variation is also shown in Fig. 3.15. This can perhaps be explained by different values of junction reactances when x_1 is varied. It is interesting to note that x_2 is always greater than x_1 (both x_1 and x_2 being less than A/2), i.e., the input port is always closer to the corner (see Fig. 3.13). Also we may note that the design curve of Fig. 3.15 can be approximately obtained by replacing either x_2 by $a-x_2$ or x_1 by $a-x_1$.

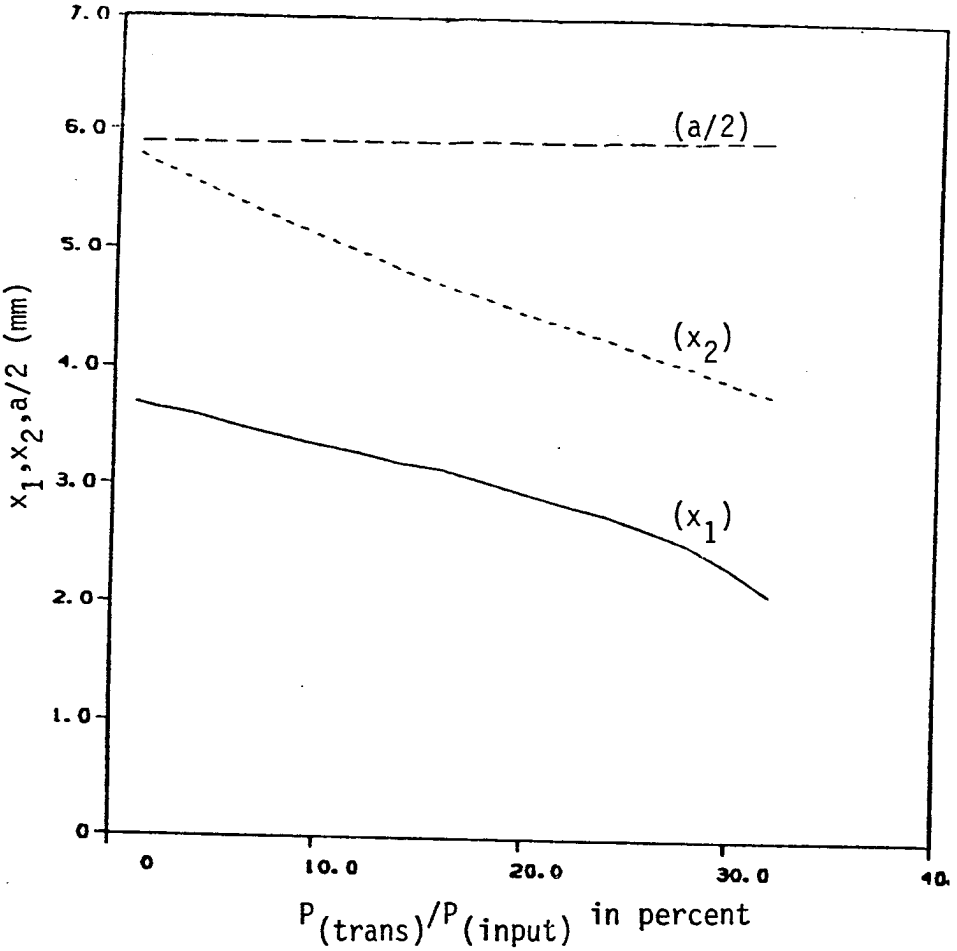

Figure 3.15 Variation of transmitted power to port 2 with the relative location of external ports and the antenna length.

b) Variation of the transmitted power with the antenna width.

Figure 3.16 shows the variation of the transmitted power with the antenna width (b in Fig. 2.7). As the antenna gets narrower the radiated power decreases so the power transmitted to port 2 increases. The resonant length, which depends on the effective dielectric constant, increases with decreasing antenna width.

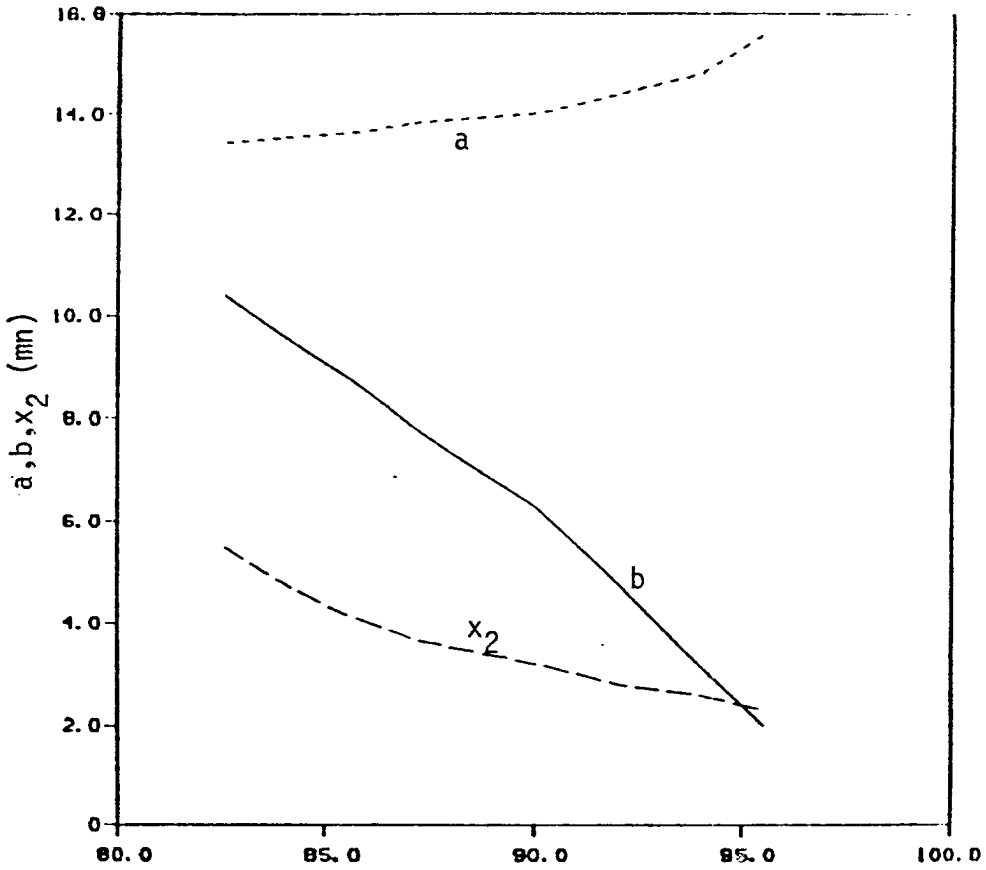

f = 7.5 GHz $\quad\quad$ δ = 0.002

ε_r = 2.48 $\quad\quad$ x_1 = 0.21 cm

h = 1/32 in.

Figure 3.16 Variation of transmitted power with antenna width b.

CHAPTER IV

EXPERIMENTAL RESULTS

Some experiments are carried out to confirm the validity of the results computed using the method developed in chapter III. First, a method for measuring the dielectric constant of the substrate used is described in this chapter. The dielectric constant of the substrate must be accurately known, since it enters into the calculation of the resonant frequency. Designs of a single feed and two-port rectangular microstrip antennas are also presented.

4.1 Measurement of the Dielectric Constant of the Substrate

The dielectric substrate available for the fabrication of the single feed and the two-port rectangular microstrip antennas was 3 M Cu clad Type GT with a nominal dielectric constant of 2.5. The dielectric constant for this substrate is specified as $\epsilon_r = 2.5 \pm 0.05$. This tolerance on the dielectric constant is likely to introduce a ± 2% variation in the resonant frequency. This is twice the order of magnitude of a typical microstrip antenna bandwidth.

a) Stripline ring resonator.

The dielectric constant was measured by designing a stripline ring resonator as shown in Fig. 4.1. The substrate is

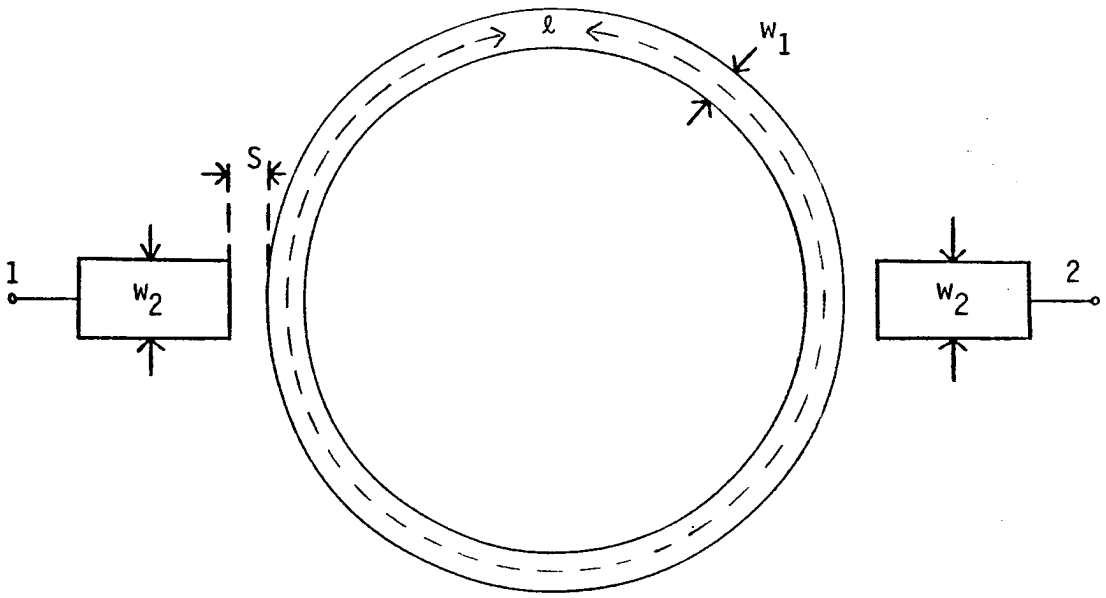

Figure 4.1 A stripline ring resonator with coupling gaps.

chosen to have a thickness of 1/32 in. The ring resonator is designed on a (2.5 in. × 2.5 in.) piece cut from the board, which is to be used in the design of the microstrip antennas. It is expected that the dielectric constant has the same value over this region of board area. The ring resonator shown in Fig. 4.1 is designed using MCAP program [11]. This configuration consists of a circular ring resonator of nominal length ℓ and width w_1 coupled to two symmetrically located transmission lines of width w_2 via gaps of width S.

The design of the stripline ring resonator is made by taking the dielectric constant of the substrate $\varepsilon_r = 2.5$. The operating frequency is chosen to be $f_r = 2.05$ GHz. The ring resonator will resonate when its length $\ell = 3.6439$ in. The width of the ring is $w_2 = 0.0101$ in., which corresponds to a nominal value of the characteristic impedance $Z_{01} = 100\ \Omega$. The transmission lines have a width $w_1 = 0.045$ in., which corresponds to a nominal value of the characteristic impedance $Z_{02} = 50\ \Omega$. The flow chart fabrication process of the ring resonator, which is also used later in the design of the antennas, is shown in Fig. 4.2. The fabrication of the stripline ring resonator was done at the integrated circuit laboratories of the Department. A photograph of the ring resonator, which was fabricated, is shown in Fig. 4.3.

b) Measurement.

The dielectric constant of the substrate is found by measuring the resonant frequency of the ring. The resonant

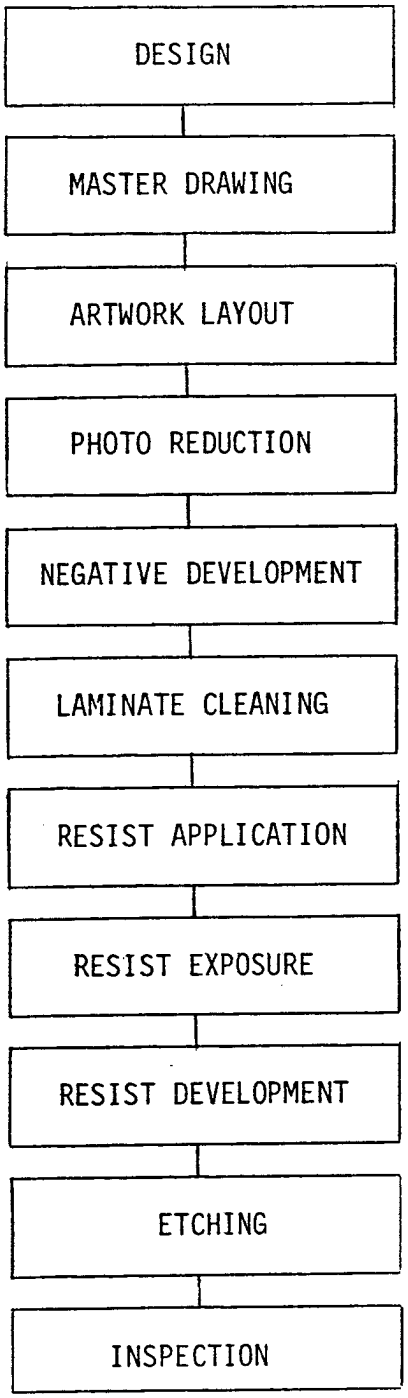

Figure 4.2 Planar Circuits and Antenna Fabrication Process

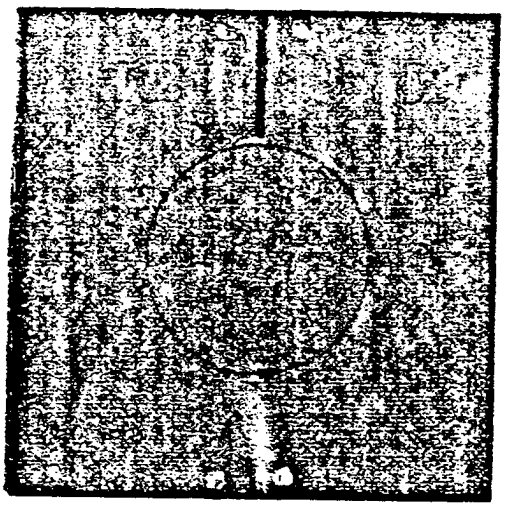

Figure 4.3 Photograph of the fabricated ring resonator.

frequency is the frequency for which the transmitted power from port 1 to port 2 (Fig. 4.1) is maximum. The setup of Fig. 4.4 was used for measuring the resonant frequency. The latter is found to be f_r = 2.058 GHz which corresponds to a measured dielectric constant $\varepsilon_r \simeq 2.48$.

4.2 Single Feed Patch

A design of a single feed rectangular microstrip patch is presented in this section. First, we will discuss the effects of uncertainties in the design parameters on the antenna performances. Then the dimensions of the fabricated antenna using the analysis of chapter III are measured and compared to the initial design parameters. The theoretical and measured performances of the fabricated antenna are finally compared.

4.2.1 Effects of parameter tolerances

It is desirable to study the effects of uncertainties in the design parameters on the antenna performances. These uncertainties are caused by fabrication tolerances, modelling approximations and measurement errors. The effects of these uncertainties on the input impedance and the resonance frequency are evaluated. The antenna, whose parameters are given in Table 3.4, is considered.

a) Effects of tolerance in ε_r

The possible uncertainty in the dielectric constant ε_r is estimated to be of the order of 0.5%. The effects of this uncertainty on Z_{in} and f_r are shown in Table 4.1. In the latter, the values of Z_{in} and f_r corresponding to $\varepsilon_r = 2.49$

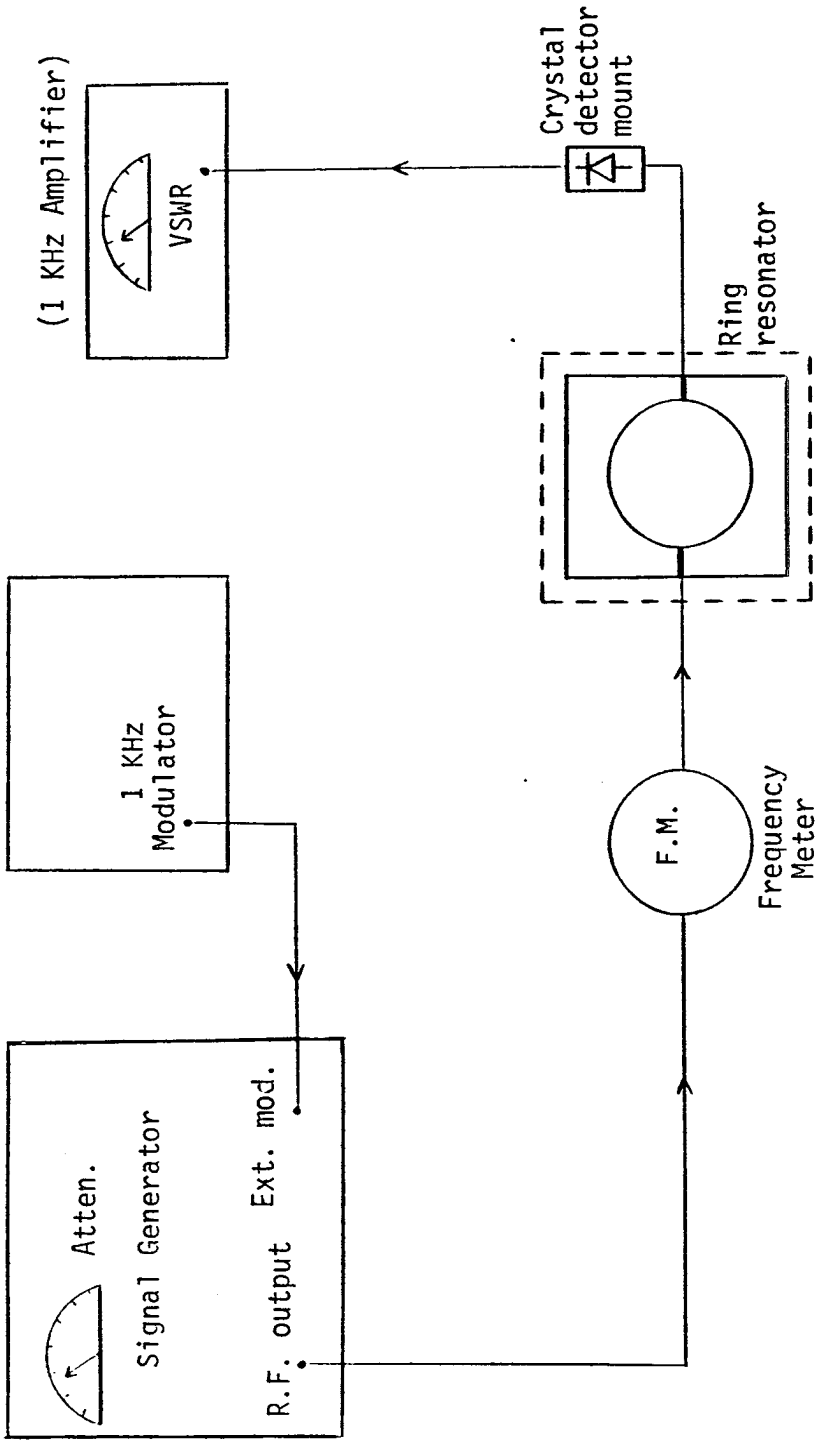

Figure 4.4 Setup for measuring the resonant frequency of the stripline ring resonator.

Table 4.1 Effects of Tolerance in ε_r on Z_{in} and f_r

ε_r	Z_{in} (Ω)	f_r (GHz)
2.47	49.13	7.513
2.48	49.53	7.500
2.49	49.60	7.481

Table 4.2 Effects of Tolerance in $(a-x_1)^*$ on Z_{in} and f_r

$(a-x_1)$(cm)	Z_{in} (Ω)	f_r (GHz)
1.16088	46.85	7.560
1.17088	49.53	7.500
1.18088	51.45	7.449

*Distance between feed point and far edge.

and $\varepsilon_r = 2.47$ are compared to their central values corresponding to $\varepsilon_r = 2.48$. Table 4.1 shows a variation of less than 2% in Z_{in} and a variation of less than 0.25% in f_r compared to their central values corresponding to $\varepsilon_r = 2.48$.

b) Effects of tolerance in antenna dimensions

A typical tolerance in the antenna dimensions a and b due to the inaccuracy in mask making and etching process, is normally of the order of 0.1 (mm). The tolerance in the antenna length a is likely to cause uncertainties in the input impedance and resonance frequency as shown in Table 4.2. This 1% tolerance in a causes a shift as large as 5.% in Z_{in} and a shift in f_r of the order of 0.8%. The results of Table 4.2 are computed by keeping the location of the feed x_1 constant. So the tolerance in a is the same as that in $(a-x_1)$, where $(a-x_1)$ is the location of the feed point to the far edge. The effects of tolerance in b on Z_{in} and f_r (as shown in Table 4.3) are less compared to those caused by the tolerance in a. This is because a is a critical parameter in the computation of the resonance frequency.

c) Effects of tolerances in the feed location.

The location of the feed point is set relative to the nearest radiating edge as shown in Fig. 3.8. A tolerance of 0.1 mm in the antenna length causes 0.05 mm uncertainty in the feed location x_1. The effects of this uncertainty on Z_{in} and f_r are shown in Table 4.4. The effects of tolerances in x_1 on Z_{in} and f_r are respectively + 1.5% and ≈ 0%. When the actual value ($x_1 = 0.31$) is less than the initial value ($x_1 = 0.315$). On the

Table 4.3 Effects of Tolerance in b on Z_{in} and f_r

b (cm)	Z_{in} (Ω)	f_r (GHz)
1.5775	50.66	7.501
1.5875	49.53	7.500
1.5975	48.33	7.495

Table 4.4 Effects of Tolerance in x_1^* on Z_{in} and f_r

x_1 (cm)	Z_{in} (Ω)	f_r (GHz)
0.310	50.4	7.500
0.315	49.53	7.500
0.320	48.30	7.497

*Distance between the feed point and nearer edge.

other hand when the actual value is $x_1 = 0.32$, there is a - 2.5% shift in Z_{in} and negligible shift in f_r.

d) Effects of tolerances in the substrate thickness.

The thickness of the substrate used is specified as (3M catalog), h = 0.0312 ± 0.003 inches. This 10% uncertainty in h causes a shift in Z_{in} of the order of 8% and a shift in f_r of the order of 0.7% so the substrate thickness is an important parameter in the design of single feed antenna at the frequency f = 7.5 GHz. These results are shown in Table 4.5.

4.2.2 Design of a single feed rectangular microstrip antenna

The method of analysis developed in chapter III is used here to determine the dimensions for a match between the feed and the patch. ε_r is taken to be equal to the measured value of 2.48. The antenna width b is taken large (b = 1.5875 cm), so as to minimize the effects of the fringing fields at the non-radiating edges. The design parameters are as follows:

- dielectric constant: $\varepsilon_r = 2.48$
- dielectric tangent loss: $\tan \delta = 0.002$
- substrate thickness: h = 1/32 in.
- resonant frequency: f = 7.5 GHz
- antenna length: a = 1.17088 cm
- antenna width: b = 1.5875 cm
- width of the 50 Ω line: w = 0.226437 cm
- thickness of the conducting strip: t = 0.7 mil ($\frac{1}{2}$ oz. copper)
- location of the feed port: $x_1 = 0.31533$ cm

Table 4.5 Effects of Tolerance in h on Z_{in} and f_r

h (mm)	Z_{in} (Ω)	f_r (GHz)
0.720	53.69	7.546
0.794	49.53	7.500
0.870	45.04	7.447

Table 4.6 Comparison between Theoretical and Measured Dimensions of the Single Feed Patch

Antenna dimensions	Design	Measurement
a (cm)	1.17088	1.1550
b (cm)	1.58750	1.5700
x_1 (cm)	0.31533	0.3050
w_{50} (cm)	0.22644	0.2150
h (cm)	0.79375	0.7620

The computed $Z_{in} = 49.53\ (\Omega)$.

The antenna configuration is shown in Fig. 4.5. The variation of the magnitude of the reflection coefficient S_{11} with frequency is shown in Fig. 4.6. At the resonant frequency $f_r = 7.5$ GHz, the computed $|S_{11}|$ is 0.008.

Figure 4.7 shows the variation of the average voltage at the radiating edges with frequency. The average voltage maximum occurs at the operating frequency $f = 8.512$ GHz, which is greater than the resonant frequency $f_r = 7.5$.

4.2.3 Measured antenna performance and comparison with theoretical values

The fabricated antenna is shown in Fig. 4.8. The first step in the analysis of this antenna is measuring its dimensions. These measurements are needed for a valid comparison of computed and measured performances. Table 4.6 shows a comparison between the designed dimensions and the measured ones. The differences are most likely to arise from the etching process. The measurement of the antenna dimensions is done using a microscope.

The antenna performances are measured using the 'Network Analyzer'. A general setup for the use of the 'Network Analyzer' is shown in Fig. 4.9. Table 4.7 shows a comparison between the computed Z_{in} and f_r using the measured dimensions and the analysis of chapter III and the measured Z_{in} and f_r using the 'Network Analyzer'. The comparison shows a good agreement between the theoretical and the measured input impedance, but a shift of + 1.4% in the resonant frequency does occur. Fig. 4.10 shows a

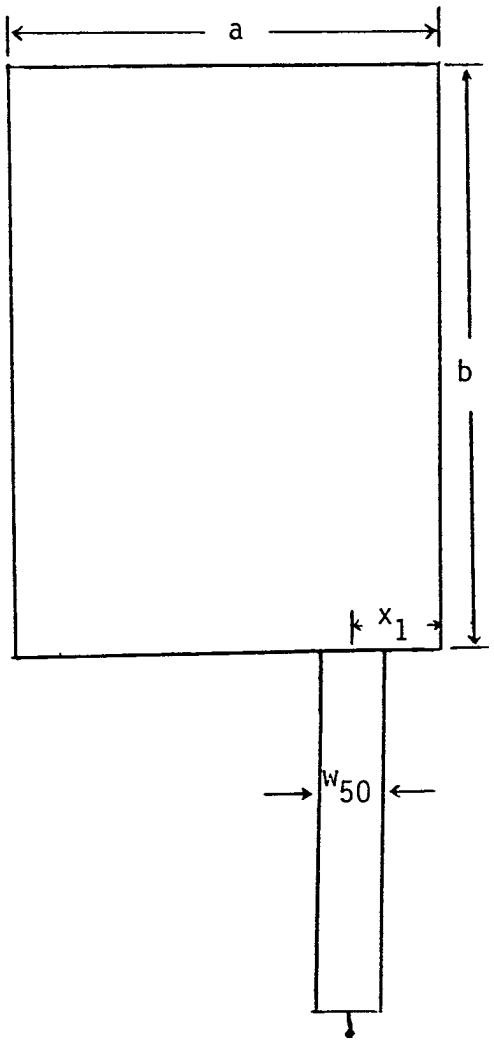

Figure 4.5 Single feed rectangular patch configuration.

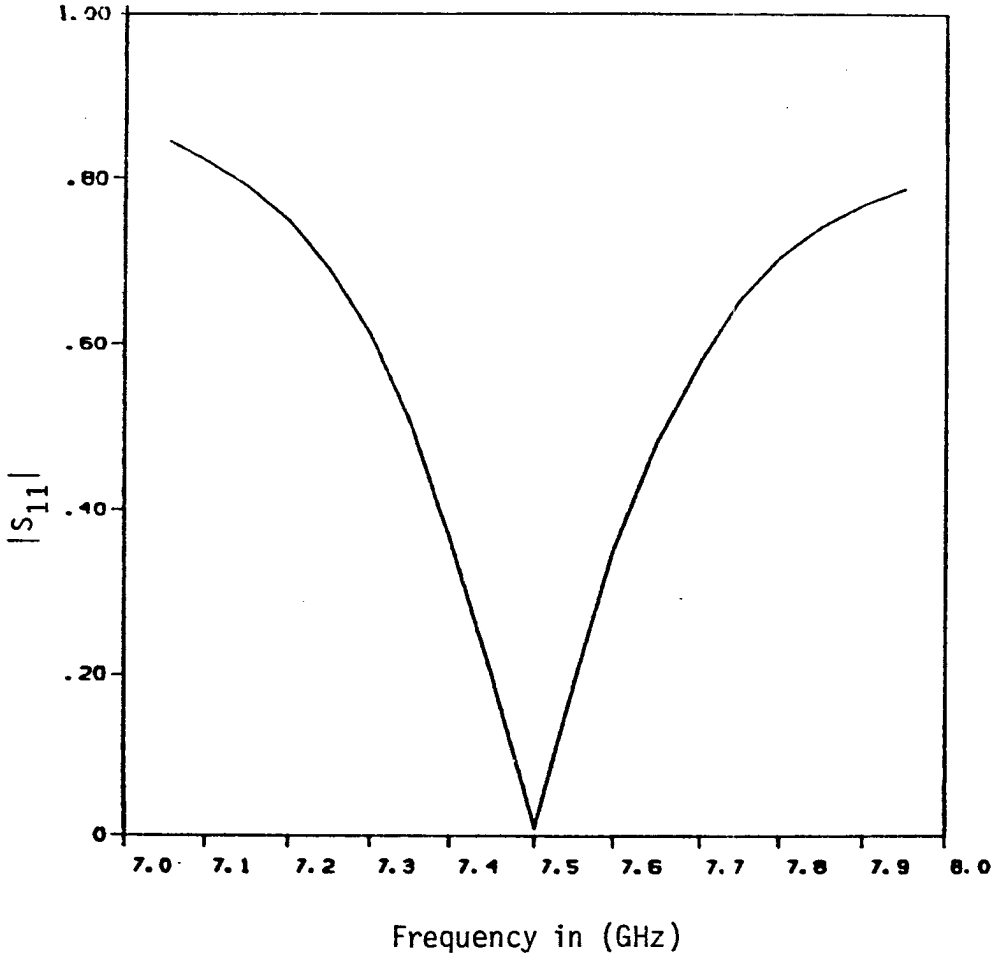

Figure 4.6 Variation of the reflection coefficient magnitude with frequency.

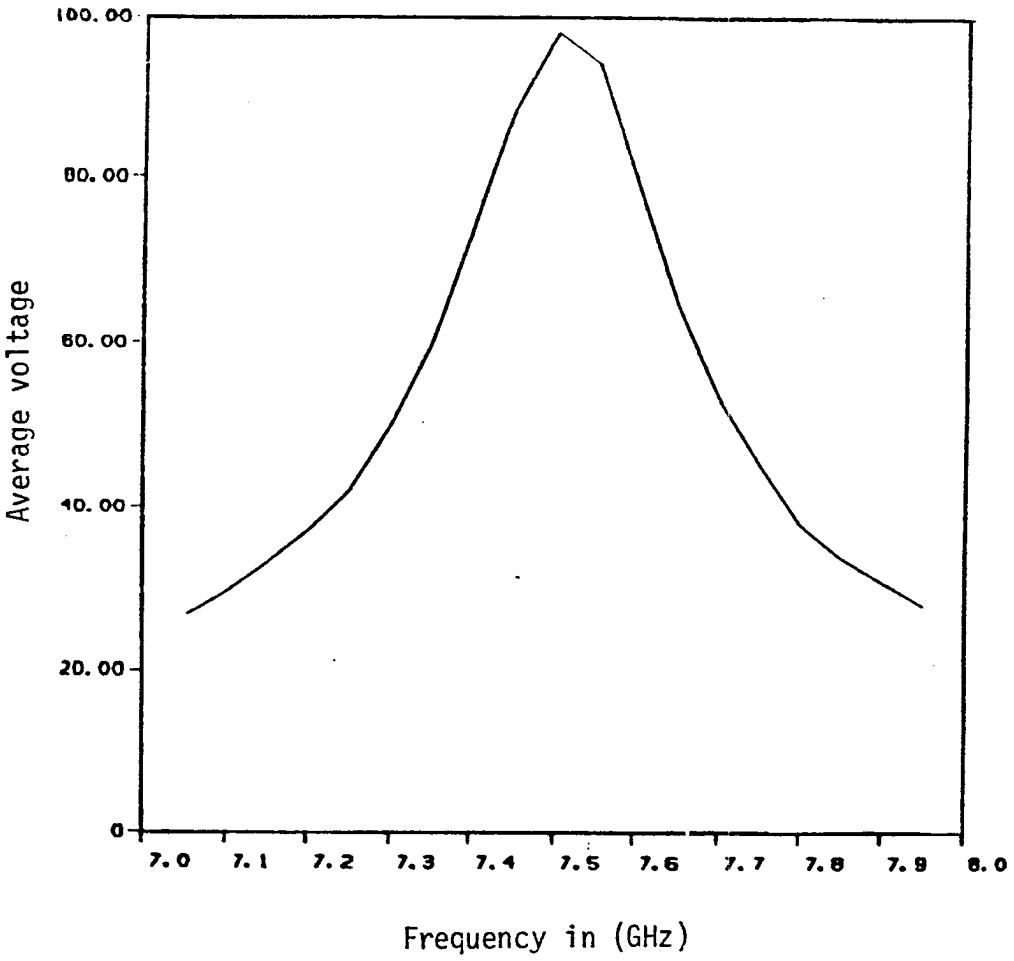

Figure 4.7 Variation of the average voltage at the radiating edges versus frequency.

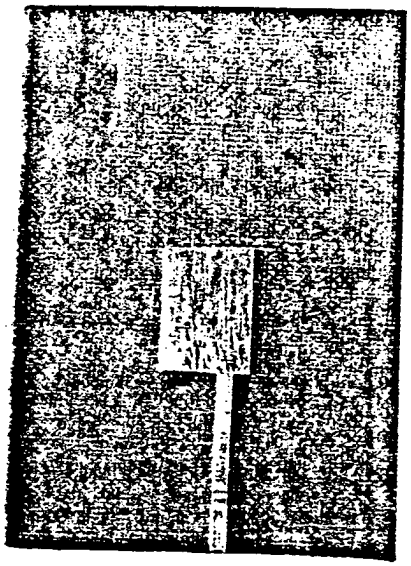

Figure 4.8 Photograph of the fabricated single feed rectangular microstrip antenna.

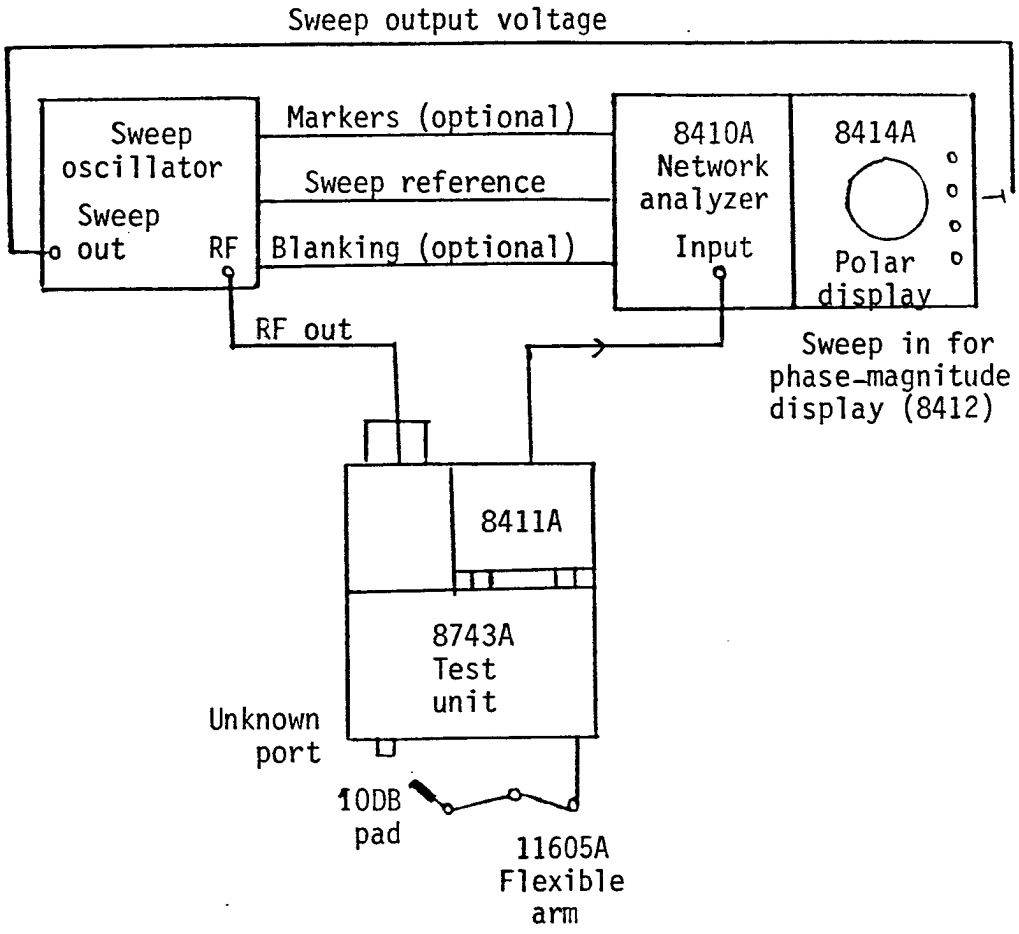

Figure 4.9 General setup for using the network analyzer.

Table 4.7 Comparison of Theoretical and Measured Z_{in}, f_r and $|S_{11}|$

	Theory	Experiment
Z_{in} (Ω)	51.7	51.2
f_r (GHz)	7.618	7.725
$\|S_{11}\|$	0.017	0.012

comparison between the variation of computed and measured reflection coefficient magnitude with frequency. The comparison shows a measured bandwidth of 3.5% which is larger than the theoretical value of 2.5%. This is partially due to neglecting the conductor losses in our analysis. Fig. 4.10 shows a good agreement between the theoretical and measured reflection coefficients, particularly at and near resonance. The slight discrepancy between the theoretical and measured $|S_{11}|$ far from resonance, may be reduced by taking more ports at the radiating edges in the analysis of chapter III.

4.3 Two-Port Patch

The design of a two-port rectangular microstrip patch using the method of analysis of chapter III is presented. The effects of uncertainties in the antenna parameters are also included. This section is concluded by comparing the theoretical and measured antenna performances (input impedance, resonant frequency, bandwidth,...).

4.3.1 Effects of parameter tolerances

The effects of uncertainties in the design parameters of a two-port antenna on its performances are discussed. It is interesting to know which are the critical parameters in the design of a two-port antenna, so particular care for the determination of these design parameters should be made. The actual antenna to be designed is chosen to have the same width as that of the single feed antenna, and to be fabricated on the same

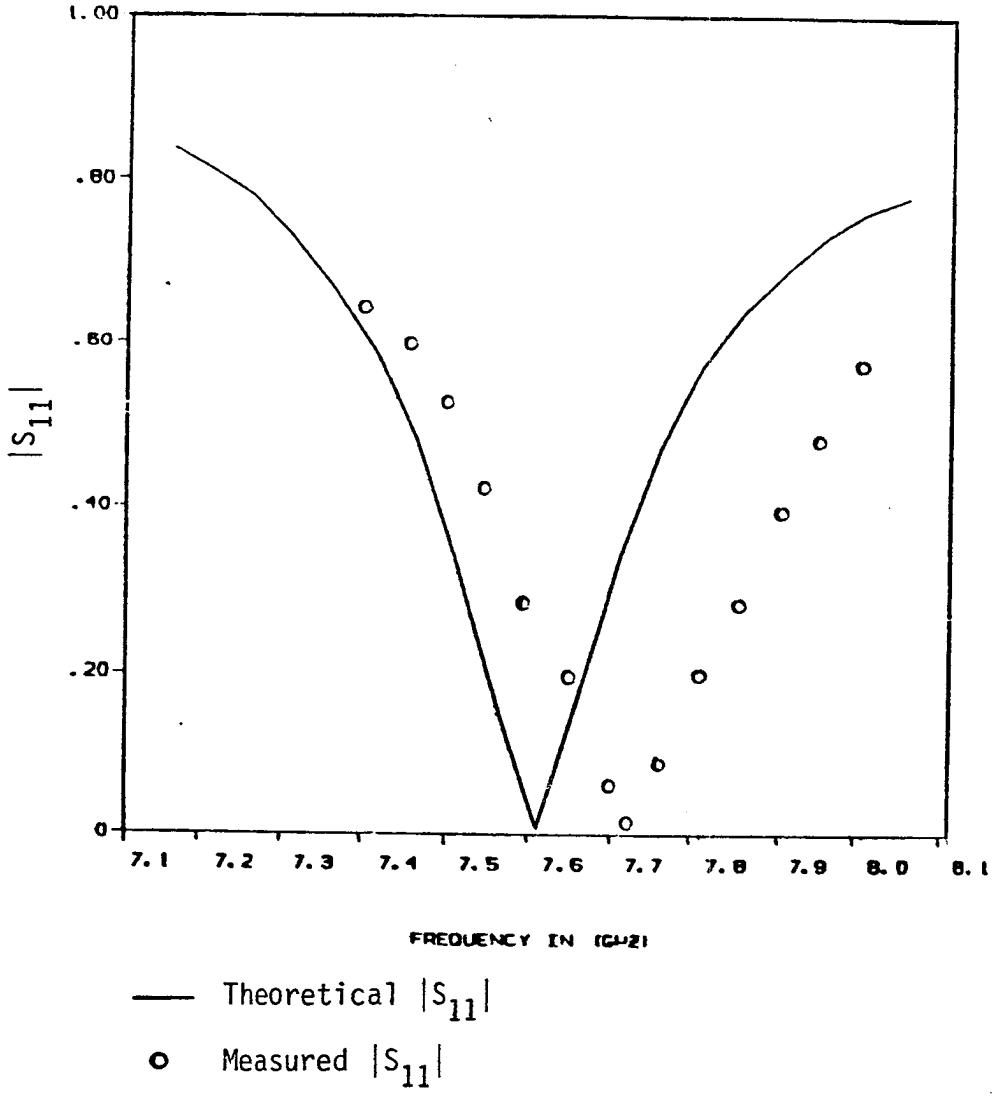

Figure 4.10 Comparison of theoretical and measured reflection coefficient magnitude.

substrate used for the latter. So the effects of the tolerances in h and b will not be repeated here. The antenna whose parameters are given in Table 3.5 is considered.

a) Effects of tolerance in ε_r.

Table 4.8 shows the effects of tolerance in ε_r on Z_{in} and f_r. A decrease (increase) of 0.5% in ε_r causes an approximate 0.18% increase (decrease) in f_r, but a negligible shift in Z_{in}.

b) Effects of tolerance in a.

Table 4.9 shows that a decrease (increase) of 0.1 mm in the value of 'a' causes an increase of .77% in f_r and approximately 2.25% change in Z_{in}. These results show that the antenna length is a critical parameter in the determination of Z_{in} and f_r.

c) Effects of tolerances in input and output port locations.

It can be inferred from Table 4.10 and 4.11 that the tolerances in x_1 (location of input port) and in x_2 (location of output port) have opposite effects on Z_{in} and f_r. In fact when both x_1 and x_2 decrease (increase), the effect of x_1 is to increase (decrease) both Z_{in} and f_r whereas the effect of x_2 is to decrease (increase) both Z_{in} and f_r. This phenomenon is much like tuning the antenna.

4.3.2 Design of a two-port rectangular microstrip antenna

The two-port rectangular patch shown in Fig. 4.11 is designed using the analysis of chapter III. The resonant length

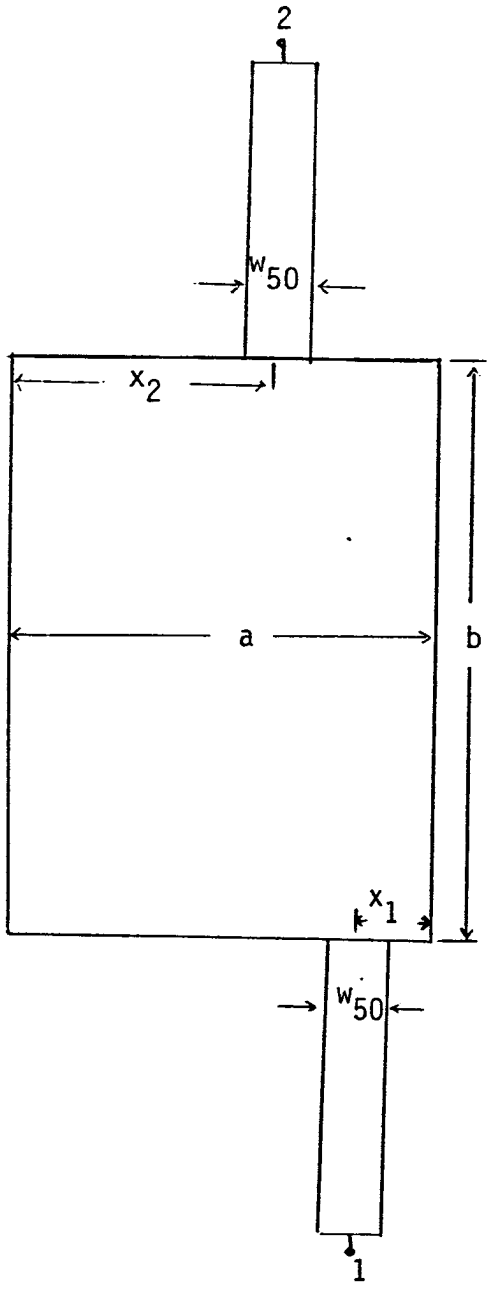

Figure 4.11 Two-port rectangular microstrip antenna.

Table 4.8 Effects of Tolerance in ε_r on Z_{in} and f_r

ε_r	Z_{in} (Ω)	f_r (GHz)
2.47	50.52	7.513
2.48	50.67	7.500
2.49	50.91	7.488

Table 4.9 Effects of Tolerance in a on Z_{in} and f_r

a (cm)	Z_{in} (Ω)	f_r (GHz)
1.17162	49.56	7.558
1.18162	50.67	7.500
1.19162	51.82	7.443

Table 4.10 Effects of Tolerance in x_1 on Z_{in} and f_r

x_1 (cm)	Z_{in} (Ω)	f_r (GHz)
0.29	53.01	7.508
0.30	50.67	7.500
0.31	47.79	7.488

Table 4.11 Effects of Tolerance in x_2 on Z_{in} and f_r

x_2 (cm)	Z_{in} (Ω)	f_r (GHz)
0.4453	48.73	7.497
0.4553	50.67	7.500
0.4653	52.6	7.503

is found by assuming the output port 2 is terminated in its characteristic impedance. The location of the input port x_1 is set equal to 0.3 mm. This value of x_1 is chosen, so the feed is not located at the corner of the patch. The design parameters are:

- dielectric constant: $\varepsilon_r = 2.48$
- substrate thickness: $h = 1/32$ in.
- conductor thickness: $t = 0.7$ mil ($\frac{1}{2}$ oz copper)
- dielectric loss tangent: $\delta = 0.002$
- operating frequency: $f = 7.5$ GHz
- antenna width: $b = 1.5875$ cm
- antenna length: $a = 1.18162$ cm
- input port location: $x_1 = 0.3$ cm
- output port location: $x_2 = 0.45527$ cm
- 50 Ω transmission line width: $w_{50} = 0.22643$ cm

The computed input impedance is $Z_{in} \doteq 50.67$ Ω.

The variation of the reflection coefficients at both the input and output ports are shown in Fig. 4.12. The transmission coefficient from port 1 to port 2 is also included in Fig. 4.12.

4.3.3 Measured antenna performances and comparison with theoretical values

The fabricated two-port antenna is shown in Fig. 4.13. Using a microscope, the measurements of the antenna dimensions were carried out. Table 4.12 shows a comparison between the initial antenna dimensions and the measured ones. Using the measured antenna dimensions, the theoretical and measured Z_{in},

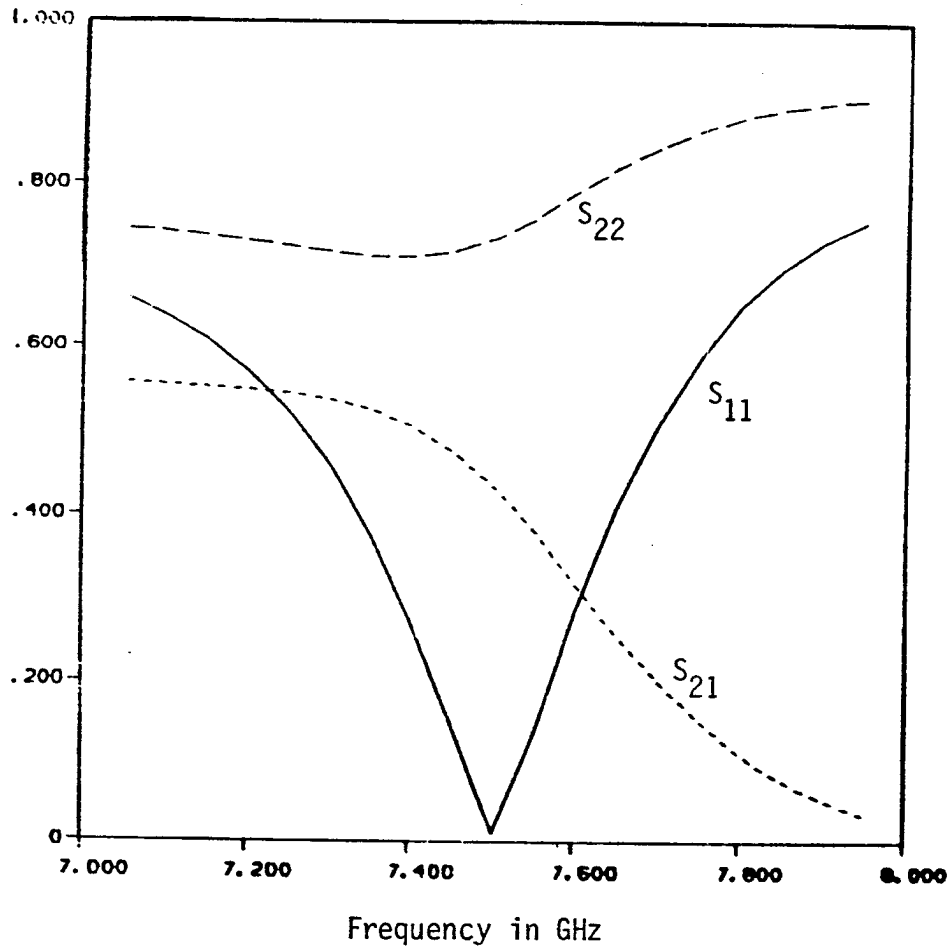

Figure 4.12 Variation of $|S_{11}|$, $|S_{21}|$, $|S_{22}|$ with frequency for a two-port rectangular microstrip antenna.

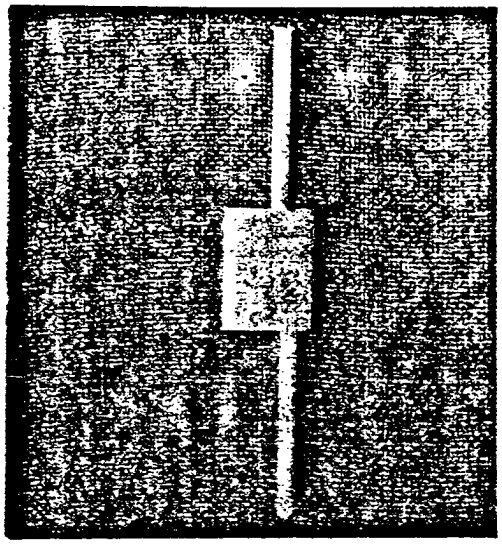

Figure 4.13 Photograph of the fabricated two-port rectangular microstrip antenna.

Table 4.12 Comparison between Theoretical and Measured Antenna Dimensions

Antenna dimensions	Theory	Measurement
a (cm)	1.18162	1.1450
b (cm)	1.5875	1.5550
x_1 (cm)	0.3000	0.2900
x_2 (cm)	0.45527	0.4470
w_{50} (cm)	.22644	0.2150
h (mm)	.79375	0.7620

Table 4.13 Comparison between Theoretical and Measured Z_{in}, f_r and $|S_{11}|$

	Theory	Experiment
Z_{in} (Ω)	50.7	51.2
f_r (GHz)	7.746	7.800
$\|S_{11}\|$	0.007	0.012

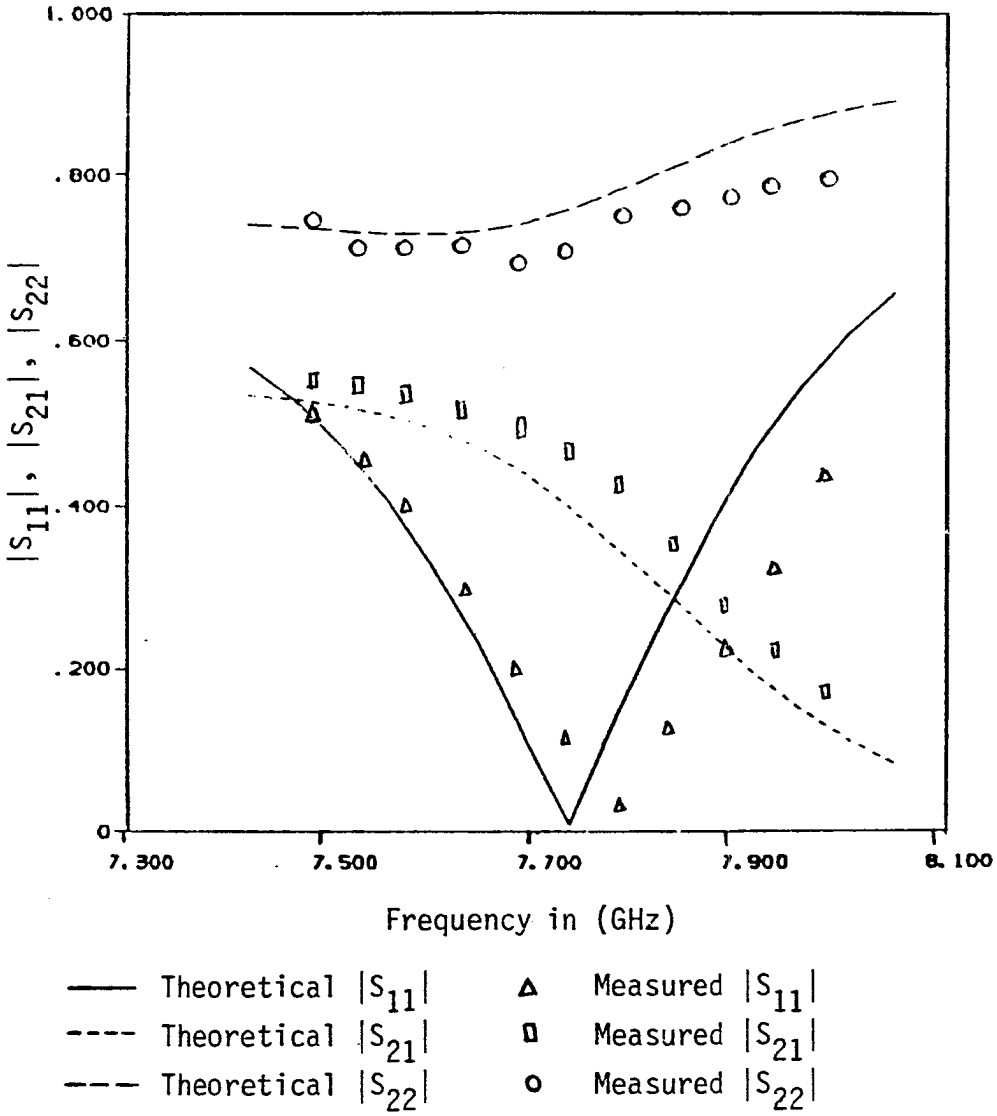

Figure 4.14. Variation of theoretical and measured $|S_{11}|$, $|S_{21}|$, $|S_{22}|$ with frequency.

f_r and magnitude of S_{11} are compared in Table 4.13. This comparison shows a good agreement in Z_{in} ($\simeq$ 1.%) and a difference of 0.69% in the resonant frequency f_r. Fig. 4.14 shows the frequency variation of the magnitude of S_{11}, S_{21} and S_{22} using both analysis of chapter III and measurement. The measured and theoretical $|S_{11}|$ and $|S_{21}|$ are in good agreement, whereas the measured values of $|S_{22}|$ are lower than those predicted by theory. The variation of measured $|S_{11}|$ with frequency shows a bandwidth of 4.3% for a VSWR $\leq$ 2. This value for the bandwidth is larger than the one predicted by theory (3.5%).

Summary

The analysis of chapter III was used to design single feed and two-port rectangular antennas. The theoretical results for the input impedance are in good agreement with the measured ones, whereas the resonant frequency predicted by theory is 1.4% lower than the measured one for a single feed patch and 0.69% lower than the measured one for a two-port patch. The analysis based on segmentation method predicts well the transmission and reflection coefficient of a two-port rectangular microstrip antenna.

CHAPTER V

CONCLUSION

The segmentation method has been used for the analysis and design of a single feed and two-port rectangular microstrip antennas.

In this analysis, an effective dielectric constant is used for the determination of the resonant frequency and an effective width for the antenna is used in the computation of the edge admittances. The effects of feed junction discontinuity are accounted for by selecting the appropriate length of the microstripline which is considered as a rectangular planar component. The values of input impedances based on this analysis are in very good agreement with the measured ones. On the other hand, for the two-port antenna the experiment shows a ~ 0.69% higher resonant frequency and a larger bandwidth compared to those predicted by theory.

The analysis reported in this thesis shows that feed line junction reactances have considerable effect on the antenna design. As seen from Table 3.1, the input impedance varies from (57.1 - j 11.9) Ω to (48.7 - j 0.04) Ω when the junction reactances are taken into account by using the segmentation method.

A significant modification of segmentation method reported in this thesis is the use of a faster algorithm for calculation

of Z-matrix of the rectangular segments. This has been explained in section (3.2.2) and is achieved by carrying out one of the summations in the Green's function analytically.

The proposed analysis can be used in the study of series feed arrays, because it gives good agreement with experiment in the determination of two-port antenna performances. The results based on the segmentation method may be made more accurate by taking into account the effects of mutual coupling between the radiating edges and also the effect of dispersion.

More experiments are under way to improve and confirm the validity of the results obtained using this model.

REFERENCES

[1] Deschamps, G.A., "Microstrip Antennas", presented at the 3rd USAF Symposium on Antennas, 1953.

[2] Bahl, I.J., P. Bhartia, "Microstrip antennas", Delham, MA: Artech House, Inc., 1980, Chapter 2.

[3] Kumar, G. and K.C. Gupta, "Trapezoidal Shaped Microstrip Antennas for Wider Bandwidth and Beamwidth", Int. Conf. Commun. Circuits and Syst., Calcutta (India), December 1981, p. 7.

[4] Sharma, P.C. and K.C. Gupta, "Analysis optimized design of single feed circularly polarized microstrip patch antennas", IEEE Trans. Antennas Propagation, Vol. AP-31, pp. 949-955, November 1983.

[5] Kumar, G. and K.C. Gupta, "Broad-Band Microstrip Antennas Using Additional Resonators Gap-Coupled to the Radiating Edges", IEEE Trans. on Ant. and Prop., Vol. AP-32, No. 12, December 1984.

[6] J.R. James, et al., "Microstrip Antenna Theory and Design", Stevenage, U.K.: Peter Peregrinus, 1981, p. 88.

[7] Van De Capelle, A., et al., "A Simple Accurate Formula for the Radiation Conductance of a Rectangular Microstrip Antenna", 1981 A.P. Int. Symp. Digest, p. 23.

[8] Kuester, E.F., et al., "The Thin-Substrate Approximation for Reflection from the End of a Slab-Loaded Parallel-Plate WG with Appl. to Microstrip Patch Ant.", IEEE Trans. Antennas and Prop., Vol. AP-30, No. 5, September 1982.

[9] Gogoi, A. and K.C. Gupta, "Wiener Hopf Computation of Edge Admittances for Microstrip Patch Radiators", AEU, Vol. 36, 1982, pp. 464-67.

[10] Wolff, I., N. Knoppik, "Rectangular and Circular Microstrip Disk Capacitors and Resonators", IEEE Trans. MIT, Vol. MTT-22, No. 10, October 1974.

[11] Gupta, K.C., et al., "Computer-Aided Design of Microwave Circuits", Delham, MA: Artech House, Inc., 1981.

[12] Gradshteyn, I.S. and I.M. Ryzhik, "Table of Integrals, Series and Products", Academic Press, 1980, pp. 40-41.

[13] Chadha, R. and Gupta, K.C., "Segmentation method using impedance matrices for analysis of planar microwave circuits", IEEE Trans. Microwave Theory Tech., Vol. MTT-29, January 1981, pp. 71-74.

[14] Fidler, J.K. and C. Nightengale, "Computer Aided Circuit Design", Middlesex: Thomas Nelson and Sons Ltd., Chapter 7, 1978, pp. 218-221.

[15] Gupta, K.C., "Two-Dimensional Analysis of Microstrip Circuits and Antennae", IETE, Vol. 28, No. 7, 1982, pp. 346-364.

APPENDIX A

Consider the Green's function given by (3.8) as

$$G(x_p,y_p|x_q,y_q) = \frac{j\omega\mu d}{ab} \sum_{m=0}^{\infty} \sum_{n=0}^{\infty} \sigma_n\sigma_m \cdot \frac{\cos(k_x x_p)\cos(k_x x_q)\cos(k_y y_p)\cos(k_y y_q)}{k_x^2 + k_y^2 - k^2} \tag{A.1}$$

This may be rewritten (separating the $n = 0$ term) as:

$$G(x_p,y_p|x_q,y_q) = C \left\{ \sum_{m=0}^{\infty} \sigma_m \frac{\cos(k_x x_p)\cos(k_x x_q)}{k_x^2 - k^2} + \sum_{m=0}^{\infty} \sigma_m \cos(k_x x_q)\cos(k_x x_p) S(m) \right\} \tag{A.2}$$

where

$$C = \frac{j\omega\mu d}{ab} \tag{A.3}$$

and $$S(m) = 2 \sum_{n=1}^{\infty} \frac{\cos(k_y y_p)\cos(k_y y_q)}{k_x^2 + k_y^2 - k^2} \tag{A.4}$$

or

$$S(m) = \left(\frac{b}{\pi}\right)^2 \sum_{n=1}^{\infty} \frac{\cos\left[\frac{n\pi}{b}(y_p+y_q)\right] + \cos\left[\frac{n\pi}{b}(y_p-y_q)\right]}{n^2 + \frac{b^2}{\pi^2}(k_x^2 - k^2)} \tag{A.5}$$

The summation (A.5) is carried out analytically using trigonometric Fourier series [12] as:

$$S(m) = -\frac{b^2}{\pi^2 \alpha_m^2} + \frac{b^2}{2\pi\alpha_m} \frac{\cosh \alpha_m(\pi-x_1) + \cosh \alpha_m(\pi-x_2)}{\sinh (\alpha_m \pi)} \tag{A.6}$$

where

$$\alpha_m = \pm \frac{b}{\pi} \sqrt{k_x^2 - k^2} \tag{A.7}$$

$$x_1 = \pi \frac{(y_> + y_<)}{b}, \quad x_2 = \pi \frac{(y_> - y_<)}{b} \tag{A.8}$$

$$y_> = \max(y_p, y_q), \quad y_< = \min(y_p, y_q) \tag{A.9}$$

Using (A.6) we can rewrite Green's function in the following symmetrical form by substituting $\alpha_m = \pm j \frac{b}{\pi} \gamma_\ell$ and using as a dummy variable which could be m or n:

$$G(x_p, y_p | x_q, y_q) = -CF \sum_{\ell=0}^{\infty} \sigma_\ell \cos(k_u u_p) \cos(k_u u_q) \frac{\cos(\gamma_\ell Z_>) \cos(\gamma_\ell Z_<)}{\gamma_\ell \sin(\gamma_\ell F)} \tag{A.10}$$

where

$$F = \begin{cases} b, & \ell = m \\ a, & \ell = n \end{cases} \tag{A.11}$$

$$(u_p, u_q) = \begin{cases} (x_p, x_q), & \ell = m \\ (y_p, y_q), & \ell = n \end{cases} \tag{A.12}$$

$$\gamma_\ell = \pm \sqrt{k^2 - k_x^2} \tag{A.13}$$

$$k_u = \begin{cases} \frac{m\pi}{a}, & \ell = m \\ \frac{n\pi}{b}, & \ell = n \end{cases} \tag{A.14}$$

$$(Z_>, Z_<) = \begin{cases} (y_> - b, y_<), & \ell = m \\ (x_> - a, x_<), & \ell = n \end{cases} \tag{A.15}$$